# POLITECNICO DI TORINO

## Master's Thesis


# Ultrasonic Fatigue Tests On Butt-Joints With Adherends Made Of Different Materials

**SAMER MAJED S294220**

**PROF.ANDREA TRIDELLO**

**PROF.CARLO BOURSIER NIUTTA**

**PROF.DAVIDE SALVATORE PAOLINO**

*Academic Year 2024-2025*

# Acknowledgements

Thanks to the tremendous help and advice of several people, writing my thesis has been an important and fulfilling experience. I would like to take this opportunity to sincerely thank everyone who contributed to this process by lending their knowledge, support, tolerance, and time. It was both an intellectual and a personal challenge to finish this work, and I could not have done it without the support of those who stood by me.

First and foremost, I want to express my gratitude to my parents, who have supported me throughout every phase of my life since I was a young child. Their unwavering support, faith in me, and selflessness enabled me to continue my education and maintain focus even in the face of adversity. Their values guided me when I had doubts, and their encouragement gave me the strength to keep going. They owe this argument just as much as I do.

Academically, I would like to express my deepest appreciation to Professor Andrea Tridello. His technical expertise, availability, and academic guidance were essential in helping me complete this thesis successfully. He consistently provided direction when I needed clarity, and his advice pushed me to aim for a higher standard in my work. His ongoing support throughout my master's program has been invaluable, and I am sincerely grateful for his trust and patience.

I also wish to thank Professor Carlo Boursier Niutta. His help was crucial, especially regarding the numerical models, software-related work, design considerations, and structural analysis aspects of this project. His input was direct, practical, and often exactly what was needed when I felt stuck. I am very thankful for the time he dedicated to explaining details and reviewing results with me. In addition, I would like to thank Professor Davide Salvatore Paolino for his assistance and for supervising my work. His guidance, discussions, and feedback were always constructive and helped improve both the technical quality of the research and the clarity of its presentation. I am grateful to all of them not only for their scientific support but also for their human support and respect.

Additionally, I would like to thank my coworkers, lab technicians, and other students for their contributions throughout this thesis time. They assisted with testing and measurements, provided equipment and expertise, and participated in discussions. Working with them made me realize that research is a team endeavor based on communication and assistance.

Lastly, a genocidal war has been and still is being fought against my people in Lebanon during the period I worked on my thesis. It has been emotionally taxing to do an academic project while observing this situation develop. This fact has humbled me and altered my perspective on my job and obligations. I have the utmost regard for those who are directly facing the violence, for those who are suffering daily loss of safety, starvation, relocation, and death. My thoughts are with all those who died during this genocide and with the students who are unable to finish their education due to this conflict. It is also my moral obligation as an engineer to make it abundantly

evident that technological knowledge is not impartial. Every algorithm, material system, and design has the potential to either create or destroy.

To everyone who supported me academically, personally, and morally

Thank you.

## Chapter 1 Table of Contents

## Table of Equations

## Table of Figures

## List of Symbols and Abbreviations

| | |
|---|---|
| VHCF | Very High Cycle Fatigue |
| HCF | High Cycle Fatigue |
| LCF | Low Cycle Fatigue |
| IET | Impulse Excitation Technique |
| CFRP | Carbon Fiber Reinforced Polymer |
| FE | Finite element |
| FFT | Fast Fourier Transform |
| $N_f$ | Number of cycles to failure |
| RH | Relative Humidity |
| $L$ | Length |
| $\lambda$ | Wavelength of the longitudinal wave in the bar |
| $E$ | Elastic Modulus |
| $f$ | Frequency |
| $\rho$ | Density |
| $c$ | Wave speed |
| $\nu$ | Poisson's ratio |
| $\sigma$ | Stress vector |
| $\varepsilon$ | Strain vector |

# Abstract

The research on the Very High Cycle Fatigue (VHCF) is very active and not limited to tests on metallic materials. Indeed, the experimental characterization of joints has become a topic of relevant interest, especially for industrial applications. The objective of the present work is to develop a testing methodology for investigating the VHCF response of hybrid butt joints, with aluminium and composite adherends connected with an adhesively bonded butt-joint.
The experimental tests are carried out with the ultrasonic testing machine, working at a loading frequency of 20 kHz and with the specimen in resonance at this frequency. A stepwise methodology is developed. First, the dynamic behavior of a cylindrical aluminium specimen has been characterized, assessing its elastic properties by using the Impulse Excitation Technique (IET). Secondly, the elastic properties of the composite plate have been assessed with an innovative procedure based on the use of the IET.
A numerical model has been thereafter developed to assess the final geometry obtained with the hybrid joint and in resonance at 20 kHz. The stress distribution in the adhesive and its variation with the adhesive material parameters, thickness and elastic modulus have been verified. A strain gage validation has finally been carried out to validate the numerical model.

# **Chapter 1** : Introduction

Many components in mechanical engineering are subjected to cyclic loading during service. Typical examples include motor and engine components, vehicle suspension and chassis parts, train wheels and axles, track elements, bridges, medical devices, and highly stressed power plant parts such as turbine rotors and compressor disks. These parts are often required to survive more than $10^7$ load cycles, and in some applications the demanded life reaches $10^9 - 10^{10}$ cycles. These extremely high numbers of cycles can come from one of two situations: either the component experiences relatively high vibration frequency during operation, or it is simply expected to operate for a very long service life without replacement. In practice, manufacturers have long observed that even parts designed for “infinite life”, such as springs, can still fail after extremely long use in the field. Already in 1999, Bathias stated clearly that there is no true infinite life in metallic materials and that failure can still occur in the so-called “endurance” region if the number of cycles is pushed far enough[i]. Sonsino later showed that the fatigue strength of components continues to decrease at very high numbers of cycles, and that this loss of strength has direct implications for safe design[ii]. Both conclusions point in the same direction: a real fatigue limit only exists in ideal conditions, for example in the absence of microstructural inhomogeneities, internal defects, or corrosive effects. Such ideal conditions do not exist in real components[iii].

The VHCF regime is also different in terms of how damage starts. In classical HCF cracks usually initiate at the surface because of slip bands, machining marks, roughness, fretting, or contact damage. In VHCF, many metallic materials instead begin to crack internally, away from the surface, often at inclusions or micro-defects[iv]. Fractography of VHCF failures often shows so-called “fish-eye” regions and a fine granular area (FGA) surrounding the origin (**Figure 1.1**), which indicates a very slow incubation stage before the crack becomes large and propagates more quickly[v]. This interior initiation is strongly controlled by micro-defects, cleanliness, residual stress state, and sometimes environment (temperature, humidity, corrosive media), so two parts made from the same alloy can behave very differently in VHCF if their defect populations are different. This is one of the reasons why standard design based only on a nominal endurance limit can be dangerous for long-life applications.

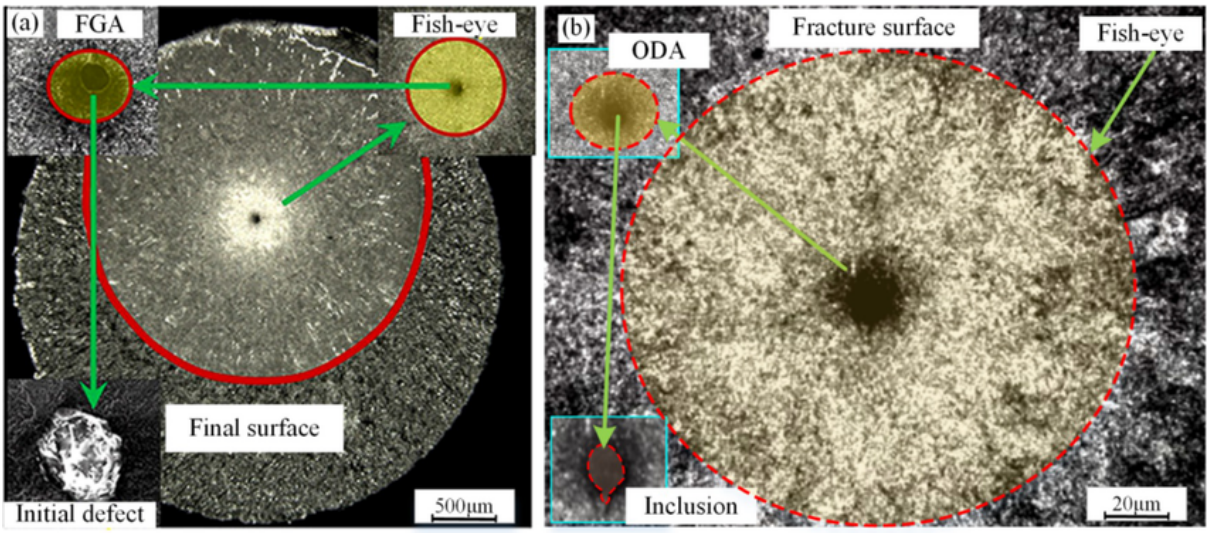


**Figure 1.1***:* Magnification of fracture surface with typical fish-eye morphology, inner FGA (ODA), and internal defect originating from the crack: (a) observed with a scanning electron microscope; (b) observed with an optical microscope. (Figure reproduced from Li et al. (2025), Fatigue & Fracture of Engineering Materials & Structures[vi]).

This VHCF problem becomes even more relevant in hybrid structures, in particular aluminum–CFRP joints and laminates. Adhesive bonding is widely adopted in aluminum–CFRP hybrid structures because it provides a continuous load path without the extra mass and local stress raisers introduced by bolts, rivets, or welds. Removing fastener holes saves weight and preserves section integrity, while a thin, well-controlled bondline spreads shear and peel more evenly so that, with proper surface preparation and a strong interface, fatigue failures tend to be cohesive within the adhesive rather than interfacial[vii]. In aluminum–CFRP joints specifically, the adhesive layer also electrically insulates the adherends and adds limited compliance to accommodate differences in elastic modulus and thermal expansion, which helps mitigate galvanic corrosion and local stress concentrations. In practice, when surface treatment, bondline thickness, and curing are controlled to specification, structural epoxies or acrylics with Young's modulus around 2–4 GPa are commonly used in automotive and aerospace applications to deliver light, durable connections [viii]. The main issue of these joints is when they are applied to high cycle load: many structural parts experience millions to billions of repeats from vibration and service loads, and bonded joints in vehicles and aircraft can enter the very high cycle fatigue (VHCF) range beyond $10^8 - 10^9$ cycles, where conventional tests at 1–50 Hz are too slow to be practical (**Table 1**). This motivates ultrasonic fatigue tests with a loading frequency close to 20 kHz[ix] . At such high loading rates, the adhesive layer may experience minor variations in stiffness, and it is essential to evaluate their effect.

| Ultrasonic Vs Conventional Fatigue Testing: | | |
|---|---|---|
| Number of cycles | Ultrasonic (20 KHz) | Conventional (1-50 Hz) |
| $10^7$cycles | 9 minutes | 1 day |
| $10^9$cycles | 14 hours | 4 months |
| $10^{10}$cycles | 6 days | 3 years |

**Table 1:** Comparison of Ultrasonic and conventional Fatigue Testing Times[x]

In this thesis, a hybrid aluminum–CFRP specimen is therefore designed to resonate in the longitudinal mode at 20 kHz. Both numerical simulations and experiments were used to adjust the design, confirming the resonance behavior.

The ultrasonic fatigue method requires the test specimen to resonate at 20 kHz in its fundamental longitudinal mode. In this study, a hybrid aluminum–CFRP joint was designed and tuned to achieve this condition, as it was the configuration selected for actual VHCF fatigue testing. FE modal analysis in LS-DYNA was employed to adjust the aluminum length until the joint's resonance matched 20 kHz, and this prediction was verified experimentally using the IET.

Besides working on a hybrid specimen, a carbon fiber specimen was introduced, where 10 pieces of carbon fiber were bonded together to study the effect of adhesive stiffness and thickness on the carbon pieces.

**Overview**: This work uses the 20 kHz ultrasonic concept mainly as a design and validation target for the hybrid aluminum–CFRP butt-joint. The tuning of distance was based on the standard half-wavelength principle for an axial resonator.

**Objectives of the Thesis**: This Master's thesis focuses on developing an experimental and numerical framework to analyze the VHCF behavior of an aluminum–CFRP bonded joint at 20 kHz. The specific objectives are:

- Design and Fabrication of Specimens: Developing both a monolithic aluminum specimen and a hybrid aluminum–CFRP adhesive joint specimen that can resonate in axial vibration at 20 kHz (ultrasonic frequency). This includes selecting geometry and materials (including an appropriate adhesive) and assembling the hybrid joint with reliable bonding.
- FEA: Creating a finite element model (using LS-DYNA) to perform modal analysis of the specimens. Tuning the model to achieve the desired resonant frequency through geometric adjustments and using it to predict mode shapes and stress distributions, particularly within the adhesive layer of the hybrid joint.
- Experimental Modal Validation: Applying the IET and strain gauge measurements to characterize the dynamic response of the specimens. Using IET to measure actual resonant frequencies and comparing them to FEA predictions for validation. Calibrating strain gauges on the specimen to correlate dynamic displacement amplitude with stress in the adhesive and validating the FE strain/stress results.

**Investigation of Key Parameters:** Through both simulation and experiment, studying the effect of critical parameters on the joint's dynamic behavior. In particular,

examining how the adhesive's stiffness and thickness, as well as the CFRP's elastic modulus, influence the resonant frequency, mode shape, and stress transfer in the hybrid joint. Identifying any optimal ranges (e.g., an ideal adhesive modulus or bondline thickness) for high-frequency performance.

# **Chapter 2** : Literature Review

## 2.1. Ultrasonic Fatigue of Hybrid joints

Previous studies have investigated whether the high loading rate used in ultrasonic fatigue affects the behavior of structural adhesives under fatigue conditions. The available evidence suggests that frequency does matter, but in a manner generally favorable for polymers. For example, Pederbelli et al.[xi] reported that a tough structural epoxy showed a higher endurance limit when tested at 20 kHz than in conventional servo-hydraulic tests at 25–50 Hz as illustrated in the figure below:

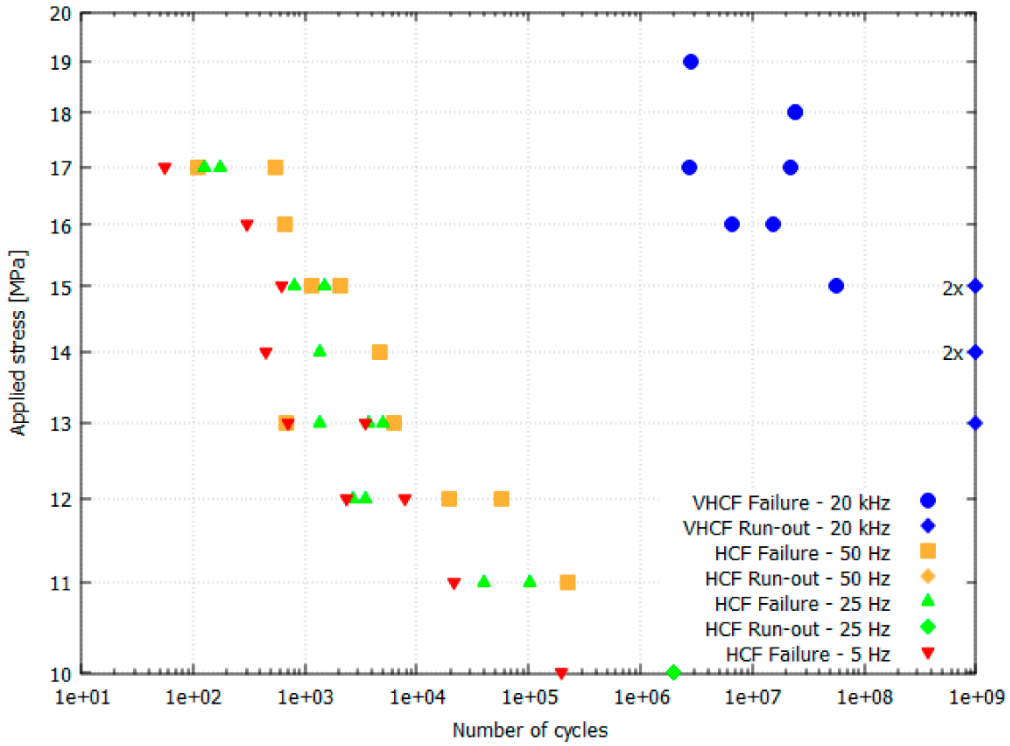


**Figure 2.1**: S-N data for an adhesively bonded cylindrical butt-joint tested at 5, 25, 50 Hz, and 20 KHz. Higher endurance at 20 KHz is evident here.[xii]

They attributed this to the simple fact that each cycle at very high frequency leaves less time for time-dependent damage such as creep, moisture-assisted degradation, or oxidation. Importantly, they also noted that the scatter of fatigue life did not increase at 20 kHz, which means the dispersion of results remained comparable to low-frequency testing. In the present thesis, we did not perform a head-to-head frequency comparison or a full endurance campaign. Instead, a hybrid aluminum–CFRP butt-joint specimen that resonates in the first longitudinal mode, close to 20 kHz, was designed and validated using modal analysis (LS-DYNA) and IET. Even so, it is relevant to note that the chosen approach using a resonant specimen at 20 kHz for

accelerated assessment is consistent with established ultrasonic fatigue practice and prior adhesive-joint studies, which together support the use of 20 kHz as a reliable and efficient route to explore durability in the gigacycle range[xiii]. Much of the current understanding of high-frequency fatigue in adhesive joints comes from the work of Tridello, Paolino, Goglio[xiv] and Pederbelli[xv], who developed and refined 20 kHz methods showing that joints can be tested at such frequencies if the geometry is tuned to resonance and temperature is controlled. Subsequent studies mapped the roles of small defects, bondline thickness, and joint geometry: even tiny voids can markedly reduce VHCF strength, while smoother geometries and fillets delay crack initiation. Overall, this literature provides a coherent picture of adhesive-joint behavior in the gigacycle regime and forms a solid basis for extending the approach to hybrid structures.

## 2.2. Literature on VHCF of Adhesive and Hybrid Joints

Most VHCF work initially focused on metals and showed that even high-strength alloys can fail well beyond $10^7$ cycles[xvi]. Building on that insight, researchers began to extend VHCF studies to other classes of materials. For structural adhesives, Tridello et al.[xvii] adapted the ultrasonic method to butt-joint specimens and ran fully reversed tension–compression tests to $10^9$ cycles on a cyanoacrylate (super-glue) joint (**Figure 2.2**). They also underline that loading frequency matters when interpreting results. For adhesives, the 20 kHz condition tends to be favorable, with reported endurance strengths that are modestly higher than at low frequency, which effectively increases the safety margin when joints are designed for very long lives.

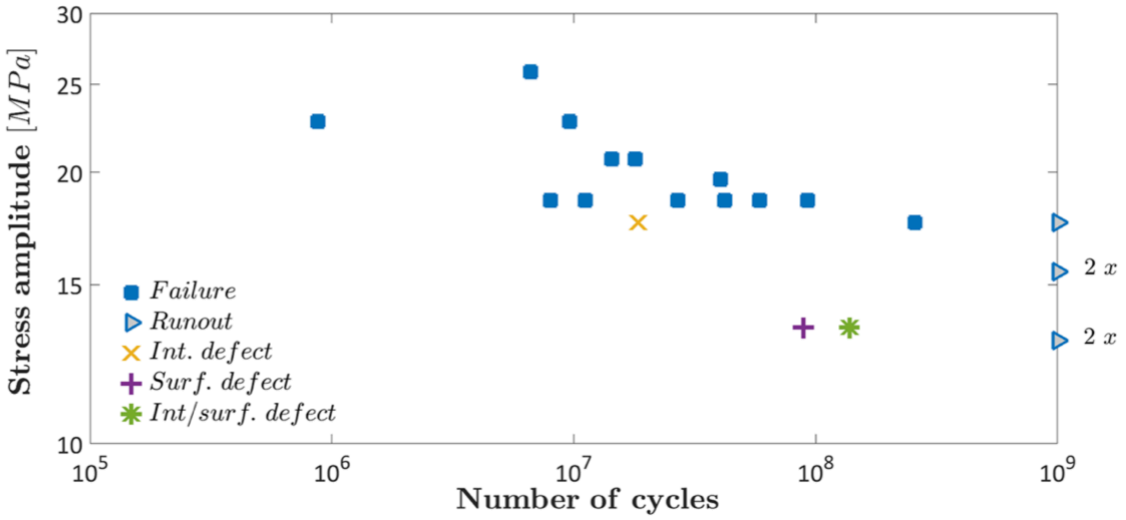


**Figure 2.2:** S–N results for cyanoacrylate butt-joint specimens tested ultrasonically at 20 kHz under fully reversed loading [xviii]

**Figure 2.2** explained that most failures happen between about $10^6$ and $10^8$ cycles at 18–26 MPa. A few samples reach $10^9$ cycles without breaking, which suggests an endurance region at the lower stresses. The symbol types show where cracks started (inside the adhesive or at the surface).

Hybrid joints, such as aluminum bonded to CFRP, bring extra complexity compared to single-material joints. The two adherends have different stiffness, thermal expansion, and surface energy. These differences affect how stresses are distributed in the adhesive and how fatigue cracks start and grow. Studies on composite–metal joints show that failure can occur either in the adhesive (cohesive) or at the interface (interfacial) (**Figure 2.3**). The result depends mainly on the surface preparation and the loading conditions. With proper treatment of the surfaces, such as abrasion, cleaning, and the use of a primer, failure usually occurs in the adhesive itself. This cohesive failure is preferred because it means the interface is stronger than the adhesive, so the measured fatigue strength is a property of the adhesive. In well-bonded joints, the adhesive properties and their defects control the joint's life, not the interface.

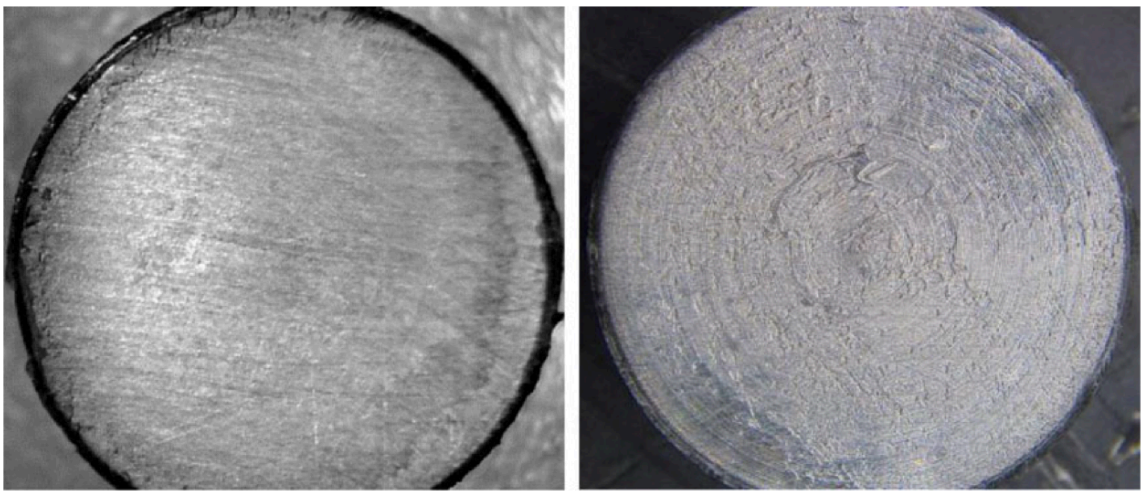


**Figure 2.3: Adherend surfaces observed by an optical microscope: A represents the cohesive failure mode and B represents the interfacial-cohesive failure mode[xix].**

The use of CFRP as one of the adherends still influences the stress state. CFRP is anisotropic and is much stiffer along the fibers than across the thickness. Under cyclic tension–compression, the CFRP part may deform differently from aluminum, for example, in terms of Poisson contraction or load sharing. Some analyses have shown that the mismatch in stiffness leads to uneven stresses in the adhesive, with higher

peel stresses near the more flexible side. The low transverse stiffness of CFRP (when fibers are aligned along the joint axis) can also increase the shear deformation of the adhesive near that side.
Despite these considerations, Perderbelli's recent results show that when the adhesive layer is thin and the bonding quality is high, the VHCF behavior of a hybrid joint is governed by the adhesive itself, rather than the large stiffness difference between aluminum and CFRP. In other words, an adhesive with a cycle endurance limit in a metal–metal joint tends to have a similar endurance limit in an aluminum–CFRP joint, as long as the joint is well-designed to avoid stress concentrations.

## 2.3. VHCF Testing Techniques and Frequency Effects

Finite element analysis is an essential tool for understanding stress distribution and dynamic behavior in joints. LS-DYNA, a flexible explicit/implicit FEA code, has been widely used for simulating complex dynamic events (crashes, impacts) and is well-suited for the high-frequency dynamic analysis in this study. As well it offers eigenvalue analysis and implicit solvers that can extract natural frequencies and mode shapes of structures. Additionally, LS-DYNA's ability to model material and interface nonlinearities (through user-defined material models, cohesive elements, etc.) makes it attractive for simulating joints under fatigue loading.
For the scope of this thesis, the focus is on using LS-DYNA for modal and dynamic analysis rather than explicit crack growth simulation. LS-DYNA's explicit solver is advantageous for simulating high-frequency resonance behavior because it can handle very short time-step oscillatory motion efficiently. Alternatively, an eigenvalue analysis (implicit) in LS-DYNA can directly compute the natural frequencies and mode shapes of the joint. In either case, the FE model must accurately represent the bonded interface. Here, a simplified approach is used, where the adhesive layer is modeled with elastic properties, assuming it remains intact (i.e., without a crack) during the modal analysis. The CFRP rods are modeled with appropriate orthotropic properties, while the aluminum is modeled with isotropic properties. Previous numerical studies provide guidance on modeling details, for example, ensuring a fine mesh in the joint is important to capture the high stress gradient across it.
In order to establish a direct link between excitation input and stress in the hybrid joint, strain gage calibration was performed under dynamic loading conditions. A highly linear stress–displacement relationship was obtained, confirming elastic behavior and enabling stresses to be expressed in physical units rather than machine parameters.

# Chapter 3 Methodology

## 3.1. Materials

Three specimen types were prepared and modeled in this section (see **Figure 3.1**): (A) an aluminum bar used as a reference, (B) a hybrid aluminum-CFRP bonded specimen, (C) a CFRP bundle specimen. Each configuration was designed and analyzed in order to understand how different materials and interfaces affect resonance.

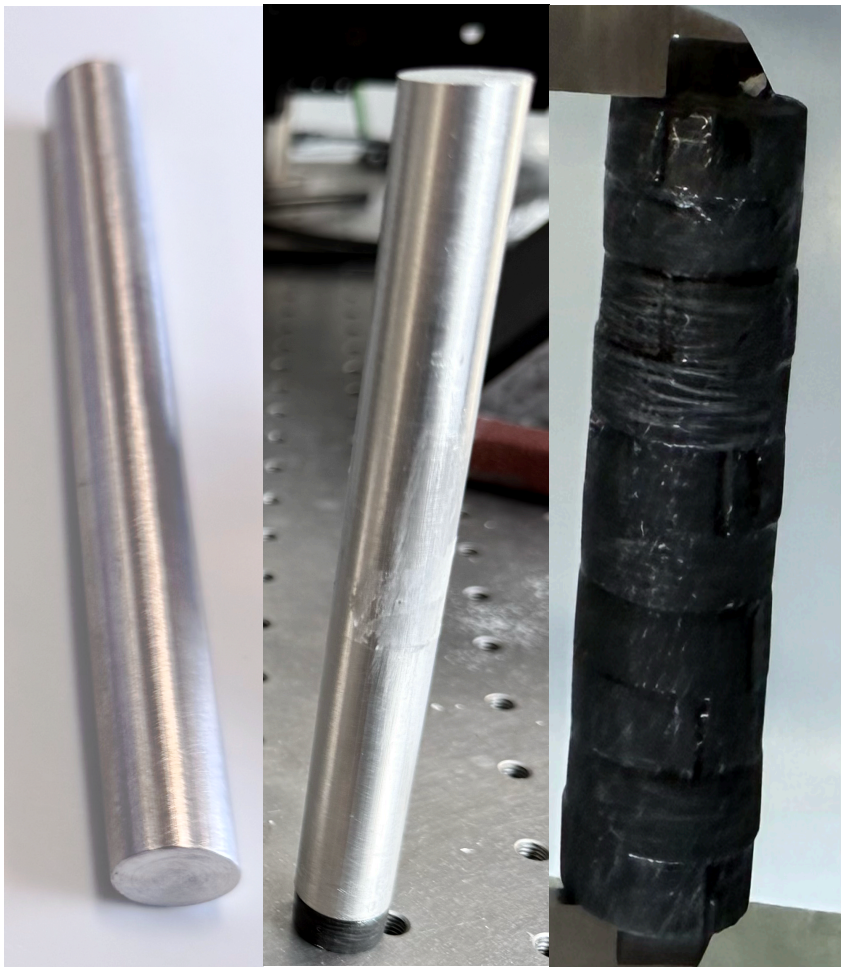

**Figure 3.1:** Specimens used in this study—(A) solid aluminum reference bar, (B) aluminum–CFRP butt-joint with thin adhesive bondline, and (C) CFRP bundle**.**

**Table 2** lists the nominal dimensions used for modeling and testing. Diameters were fixed (15 mm for the aluminum bar and hybrid, 20 mm for the CFRP bundle).

| ID | Specimen | Diameter [mm] | Length [mm] | Bondline [mm] |
|---|---|---|---|---|
| **A** | Aluminum bar | 15 | 150 | - |
| **B** | Hybrid joint | 15 | 125 | 0.08 |
| **C** | Carbon bundle | 20 | 68.71 | 0.08 |

**Table 2**: Nominal specimen dimensions.

For the FE models, aluminum and adhesive were modeled as isotropic elements, whereas CFRP was defined as an orthotropic material. The values in **Table 3** were used for all runs unless noted. The CFRP was assigned an orthotropic elastic model with a local coordinate system specified in the material definition. The local axes were rotated such that the c-axis is aligned along the bar (longitudinal) direction, with the a and b axes taken as the hoop and radial directions, respectively. After this mapping, the longitudinal modulus is $\mathrm{E_c}$, and the transverse moduli are $\mathrm{E_a}$ (hoop) and $\mathrm{E_b}$ (radial).

| Material/Layer | ρ [Kg/$m^3$] | $E_a$[GPa] (hoop) | $E_b$[GPa] (radial) | $E_c$[GPa] (along bar) | $\nu_{ba}$ [ - ] | $\nu_{ca}$ [ - ] | $\nu_{cb}$ [ - ] |
|---|---|---|---|---|---|---|---|
| **Aluminum(isotropic)** | 2700 | - | - | 72.1 | - | - | 0.3 |
| **CFRP (orthotropic-elastic)** | 1500 | 54 | 54 | 8.6 | 0.05 | 0.05 | 0.05 |
| **Adhesive(isotropic)** | 1100 | - | - | 3 | - | - | 0.35 |

**Table 3**: Materials properties used in FE models, Values for E and ν are room-temperature inputs.

## 3.2. Specimen Preparation

### 3.2.1. Carbon bundle cutting

The CFRP sheet used in the hybrid and bundle specimens were designed then cut from a flat composite sheet to the required dimensions using a waterjet cutting machine. During the process, the sheet was fully immersed in water, which helped absorb the cutting energy and reduce heat generation. This setup prevented delamination and fiber pull-out, protecting the epoxy matrix from thermal damage. The sheet was firmly clamped to keep it stable, and the feed rate was kept moderate for a clean cut. After cutting, the edges were lightly sanded to remove small irregularities and to ensure smooth surfaces for bonding.

**Figure 3.2:** The CFRP sheet while cutting the first CFRP specimen

### 3.2.2. Preparation of Carbon Rod Assemblies

The composite bundle was prepared by progressively bonding ten individual carbon rods using Loctite adhesive. Before bonding, the contact surfaces of each pair of rods were carefully cleaned with isopropanol to remove dust and grease, ensuring good adhesion. The rods were then aligned and pressed together using mechanical clamps, applying light pressure to achieve a uniform and thin adhesive layer. After joining two rods, the assembly was left for a short period to allow the adhesive to partially cure and stabilize before adding the next pair. This step-by-step approach was repeated until all ten rods were combined into a single cylindrical bundle. The use of clamps ensured that the rods remained in close contact during curing, minimizing voids and misalignment. The final assembly was left to fully cure before further machining and integration with the aluminum part.

Noting that the adhesive was allowed to fully cure (24 h at room temperature, as recommended for HY 4070 for full strength) (**Figure 3.3**)

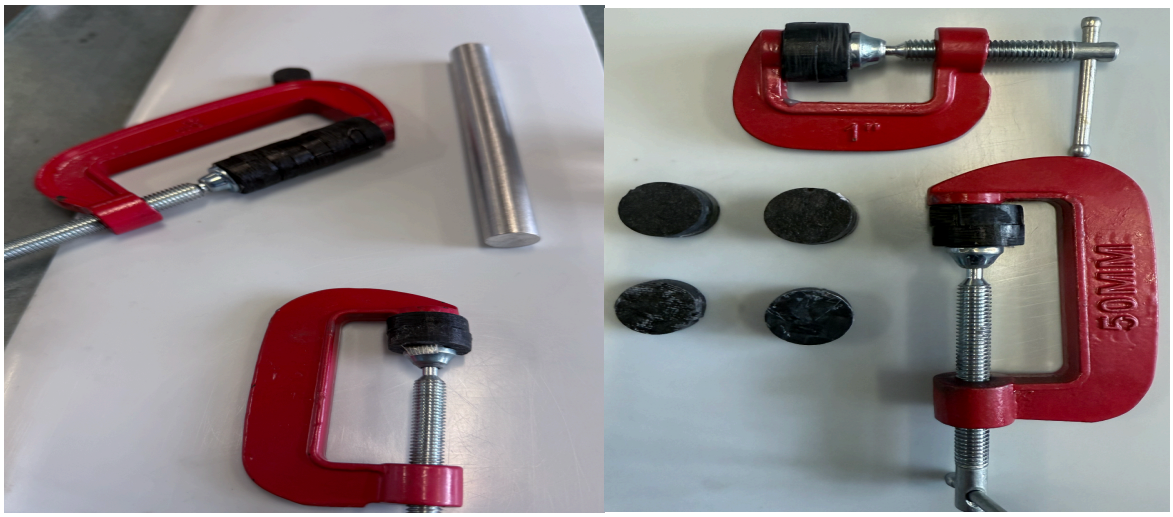


**Figure 3.3**: Preparation of carbon rod.

### 3.2.3. The hybrid specimen preparation:

The hybrid joint was produced by bonding the aluminum bar to the CFRP section using a thin layer of structural adhesive. Before bonding, the aluminum surface and the mating surface of the CFRP were both cleaned with isopropanol to remove machining residue, dust, and grease, in order to promote proper adhesion. The aluminum end face and the CFRP end face were then aligned in axial contact and brought together with a controlled, uniform bondline thickness of approximately 0.08–0.10 mm. This thickness was maintained using a clamping setup: the two parts were held in position with light mechanical pressure, not high load, so that the adhesive layer stayed continuous but was not squeezed out. Care was taken to avoid tilt between the two parts so that the contact remained perpendicular and the joint stayed coaxial. Once the adhesive was applied and the parts were clamped in place, the assembly was left undisturbed to allow the adhesive to cure and stabilize in the correct geometry. After clamping, the bonded aluminum–CFRP assembly was left to complete the full curing process. After curing, the joint was handled as a single hybrid specimen and could be machined and measured as one part. The aim of this procedure was to obtain a clean, repeatable interface with minimal voids, good alignment between the aluminum and CFRP axes, and a controlled adhesive thickness.

## 3.3. Finite Element Modal Analysis with LS-DYNA

Finite element analysis was used in designing and understanding the specimens' dynamic behavior. LS-DYNA was chosen for its ability to perform both explicit dynamic simulations and eigenvalue (modal) analysis. The modeling efforts included: modal tuning of the aluminum rod, analysis of the hybrid joint's mode shapes, and parametric studies on material properties (composite modulus, adhesive stiffness, adhesive thickness). Additionally, simulations supported the interpretation of the Impulse Excitation Technique results by providing mode shape visualization.

**Type A: Aluminum Specimen (15 mm in diameter):**

As a first step, a simple aluminum bar was modeled in LS-DYNA to establish a baseline for the dynamic behavior. The bar was meshed with solid brick elements, ensuring a regular grid along the length to capture longitudinal vibrations accurately. Material properties corresponding to aluminum were used (**Table 3**).

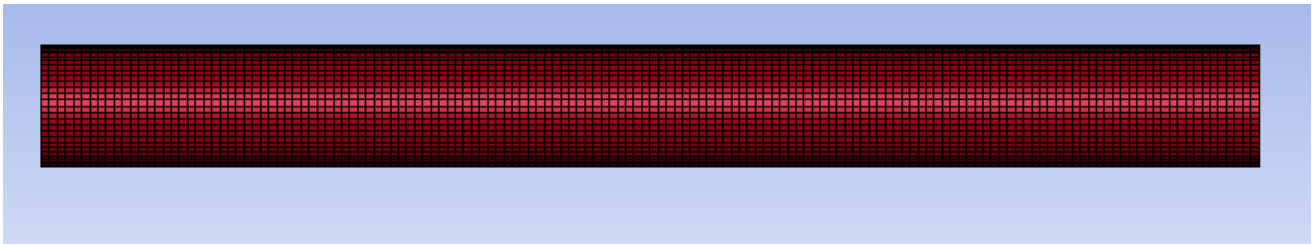

**Figure 3.4**: Aluminum bar in LS-DYNA

**Type B**: **Hybrid Aluminum–CFRP bonded specimen (15 mm diameter):**
This specimen consists of an aluminum rod adhesively bonded to a CFRP rod of the same diameter, forming a butt joint. The adhesive layer between them is a thin film that bonds the flat end of the aluminum to the flat end of the CFRP. The design philosophy was to make the total assembly behave like a uniform rod in its lowest axial mode, with the adhesive layer experiencing nearly uniform tensile stress.

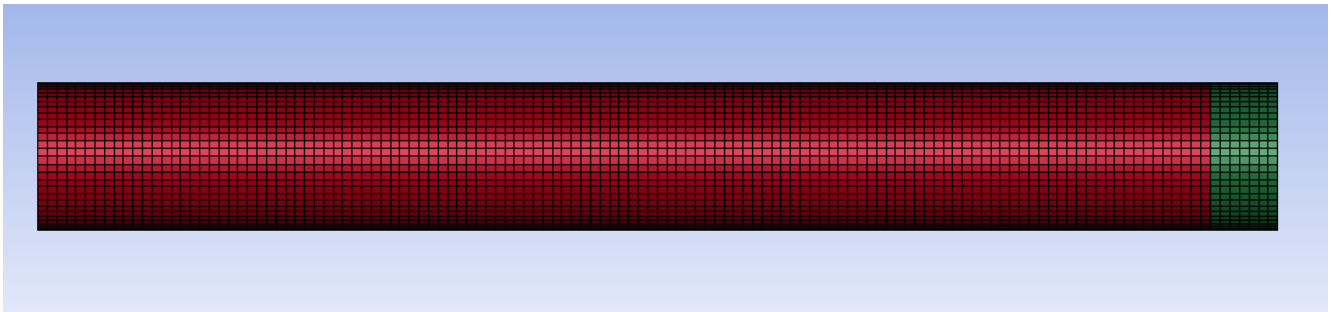

**Figure 3.5**: Finite element mesh of the hybrid specimen (aluminum in red, CFRP in green) used for modal analysis in LS-DYNA.

**Type C: CFRP Bundle Specimen (20 mm Diameter)**
The third configuration investigated was a CFRP bundle specimen, created by assembling ten carbon-fiber rods into a single bonded composite unit. The rods, each approximately 6.81 mm in length (**Figure 3.6**). Also, this bar was meshed with solid brick elements to ensure a regular grid along the length to capture longitudinal vibrations accurately.

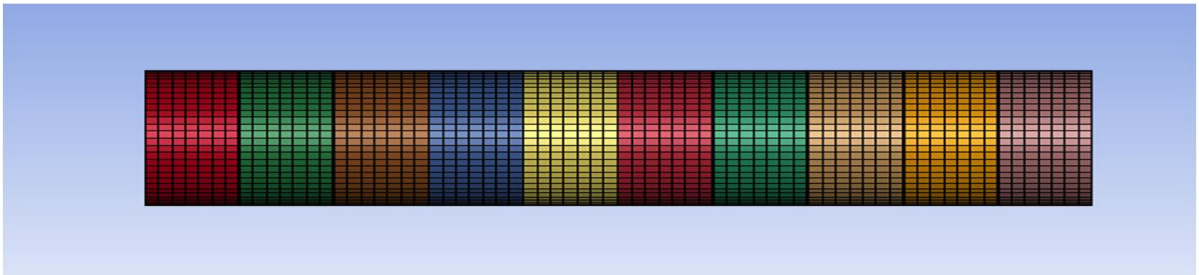

**Figure 3.6***:* 10 pieces of carbon fibers bonded together with adhesive designed in LS-DYNA

## 3.4. Specimen Length Estimation:

To obtain a specimen that resonates in the first longitudinal mode at approximately 20 kHz, an initial length estimate was made using one-dimensional wave theory. In the first step, the hybrid specimen (aluminum + adhesive + CFRP) was approximated as an equivalent free–free aluminum bar. This is acceptable as a first-order estimate because the CFRP section in the final design is very short compared to the aluminum

section, so its influence on the global axial stiffness and mass distribution is limited in the first approximation.
For a free bar vibrating in its fundamental longitudinal mode, the shape is half a wavelength. In other words, the total length L of the bar satisfies.

$$L = \frac{\lambda}{2} \quad \textbf{(1)}$$

The wavelength is related to wave speed $c$ and frequency $f$ by

$$\lambda = \frac{c}{f} \quad \textbf{(2)}$$

Combining the two relations gives the standard half-wavelength estimate for a longitudinal resonator:

$$L = \frac{c}{2f} \quad \textbf{(3)}$$

The axial wave speed in an elastic bar is given by

$$C = \sqrt{\frac{E}{\rho}} \quad \textbf{(4)}$$

Substituting values in **(4):**

$$C = \sqrt{\frac{72\times10^9}{2700}} = 5100 \text{ m/s} \quad \textbf{(5)}$$

Substituting the value of $C$ and $f = 20$ KHz, and using **(3):**

$$L = \frac{c_{Al}}{2f} = \frac{5100}{2\times20000} = 0.1275 \text{ m} = 127.5 \text{ mm} \quad \textbf{(6)}$$

This first-order analytical calculation indicates that, to resonate in the fundamental longitudinal mode at 20 KHz, the total specimen length should be on the order of 125-130 mm. Since the design of the hybrid joint includes a short CFRP segment of approximately 7 mm bonded to the aluminum, the remaining length for the aluminum portion was initially set to about 120 mm. This half-wavelength in aluminum estimate was then used as the starting geometry, before refining the design with FE modal analysis to capture the effects of the adhesive layer, the carbon segment, and the actual boundary conditions.

### 3.5.1. Free–Free Axisymmetric FE Model and Geometry Calibration for the 20 kHz Longitudinal Mode

In the finite element model, a more precise tuning was performed to lock the specimen's longitudinal resonance to 20 kHz. A 2D axisymmetric FE model (four-node axisymmetric elements) was used as the first step (see **Figure 3.7**). In this model, the aluminum bar and the CFRP segment were both assigned their respective elastic properties, and a thin adhesive layer was explicitly included between them to represent the bonded interface. The model was set up with free–free boundary conditions (no constraints at either end), in order to reproduce the behavior of a slender rod vibrating in air without external supports. The eigenvalue analysis was then used to extract the natural frequencies and the associated mode shapes of the assembly, focusing in particular on the first longitudinal mode.

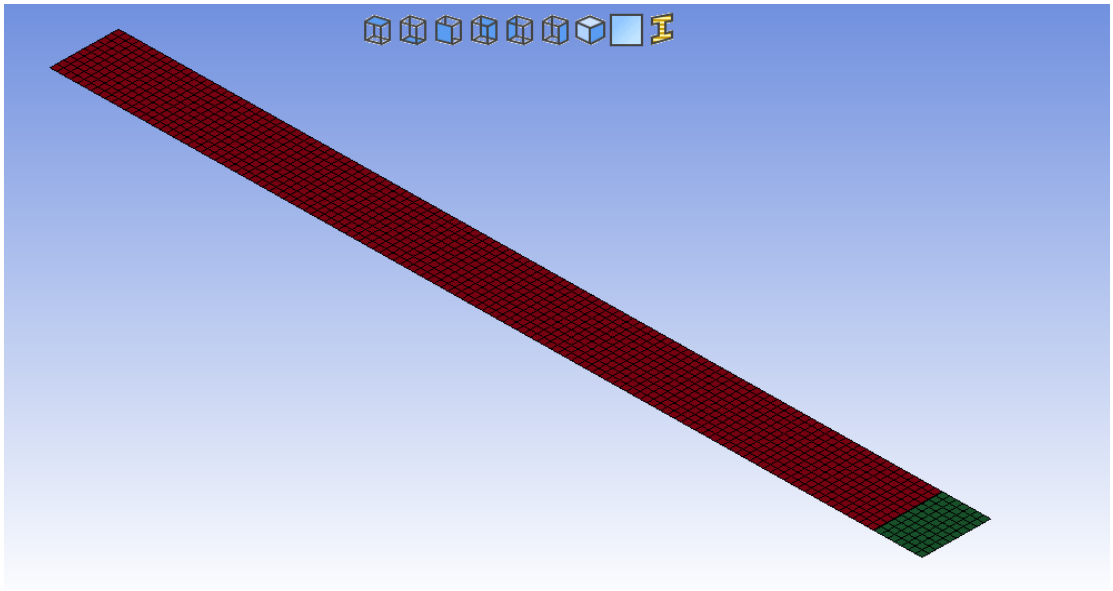

**Figure 3.7**: 2D 4 nodes shell

With this setup, the geometry was iteratively tuned. The CFRP segment length was fixed at 6.8 mm in all runs, consistent with the intended manufactured joint. The length of the aluminum bar was treated as the parameter to adjust. Starting from an aluminum length of 120 mm, the predicted fundamental longitudinal frequency was slightly too high, around 20.55 kHz. This makes sense physically: a shorter bar is stiffer and has a higher longitudinal resonance. As the aluminum length was increased in the model, the resonance frequency shifted downward (a longer bar behaves like a longer resonator, so it rings at a lower frequency). An aluminum length of about 123 mm reduced the first longitudinal mode to approximately 20.03 kHz, already close to the 20 kHz target. A further slight increase to 125 mm brought the first longitudinal mode essentially to the design target, around 20.005 kHz (i.e., within only 5 Hz of 20 kHz). This numerical tuning therefore identified the required nominal geometry for

fabrication: aluminum section length = 125 mm, CFRP section length = 6.8 mm (fixed), and an adhesive layer thickness of roughly 0.08 mm. At these values, the FE model showed a clean longitudinal mode at 20 kHz with the expected half-wavelength shape (nodes at the ends, maximum axial displacement near the free center), which is exactly the operating mode needed for ultrasonic VHCF loading.

To verify that this result was not an artifact of the simplified axisymmetric model, a full 3D finite element model of the same specimen was then generated and analyzed using the same material definitions (orthotropic CFRP, isotropic aluminum, compliant adhesive layer) and the same free–free boundary conditions. In the 3D model, the adhesive layer and the CFRP block were represented with their actual diameters and interfaces rather than an idealized revolution surface. The first longitudinal mode obtained from the 3D model was essentially the same as in the axisymmetric study, both in shape and in frequency: the fundamental axial resonance remained extremely close to 20 kHz for an aluminum length of about 125 mm and a CFRP segment of about 6.8 mm. The slight difference between the 2D and 3D predictions (on the order of a few tens of Hz at most) confirms two essential points. First, the longitudinal mode is dominant and well separated from bending or torsional modes in this geometry, so the specimen will mainly vibrate in pure axial extension/compression at the target frequency. Second, the axisymmetric model is sufficient for dimension tuning, because it already captures the correct mass–stiffness distribution of the aluminum/adhesive/CFRP stack. After this cross-check, the 125 mm aluminum length and 6.8 mm CFRP length were accepted as the final design dimensions for manufacturing and experimental validation. It is worth noting that the accuracy of material properties is essential in this tuning.

Experimental measurement (detailed in the next section) indicated that the aluminum's effective modulus was closer to 72.1 GPa, which was used in the model to improve accuracy. Similarly, the composite material's properties were initially estimated (we considered a range for the composite's through-thickness modulus $E_c$ from 5 to 20 GPa to see if it affected the results).

### 3.5.2. Mode Shape Identification:

The modal analysis of the final design (125 mm Al + 6.8 mm CFRP + adhesive) revealed several modes in the frequency range of interest. The first few modes were inspected to understand their nature (see **Figure 3.8**):

- Mode 1 (around 19 kHz) that has a side-to-side bending which appeared to be in the first bending mode.
- Mode 2 (around 19 kHz in some intermediate models) corresponds to a second bending mode, or possibly an orthogonal bending if two directions are similar – essentially, the rod vibrating laterally. In a symmetric rod, two nearly identical bending modes can occur in perpendicular planes (these often show up as degenerate modes with the same frequency).

- Mode 3 was identified as the first true axial mode (longitudinal compression/extension), which was the target mode around 20 kHz. This mode shape involves the aluminum and composite oscillating along their length, with the maximum axial stress and strain occurring near the mid-length and near the interface.

| Mode | Mode Shape | Description | Example: |
|---|---|---|---|
| **Mode 1** | Side-to-side bending | First **bending mode** (in a plane, like a beam) | 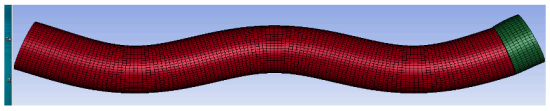 |
| **Mode 2** | Side-to-side bending (orthogonal) | Second **bending mode**, 90° to Mode 1 (degenerate due to symmetry) | 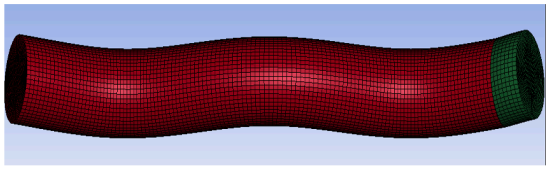 |
| **Mode 3** | Uniform compression/extension | First **longitudinal mode** — axial vibration | 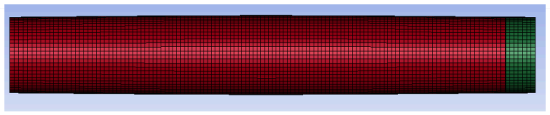 |

**Figure 3.8:** Table showing the difference between modes.

## 3.6. Experimental Validation

### 3.6.1. Impulse Excitation Technique (IET) for Dynamic Modulus and Frequency

The dynamic behavior of all specimens was characterized experimentally using the IET, a non-destructive vibration method standardized for determining elastic properties and natural frequencies from resonance data (**Figure 3.9**).

In this procedure, each specimen was supported in an approximately free–free condition and lightly excited by a mechanical tap. The resulting vibration response was measured and processed in the frequency domain using a fast Fourier transform (FFT) to identify its natural frequencies. This approach was applied to three configurations: a homogeneous aluminum cylinder, the hybrid aluminum–CFRP joint, and the CFRP bundle. For the aluminum specimen, the first longitudinal resonance was used not only to identify the modal frequency, but also to back-calculate the dynamic Young's modulus, which was found to be about 72 GPa. This modulus was then taken as the elastic stiffness input for the finite element (FE) simulations. The hybrid joint and the CFRP bundle were tested in the same way to extract their fundamental longitudinal frequencies, which were then compared with the corresponding mode predictions from LS-DYNA. The agreement between the measured resonance frequencies and the FE-predicted frequencies was very good, confirming that the numerical model (including

the aluminum section, the CFRP section, and the adhesive layer) correctly captured the effective stiffness and mass distribution of the specimens.

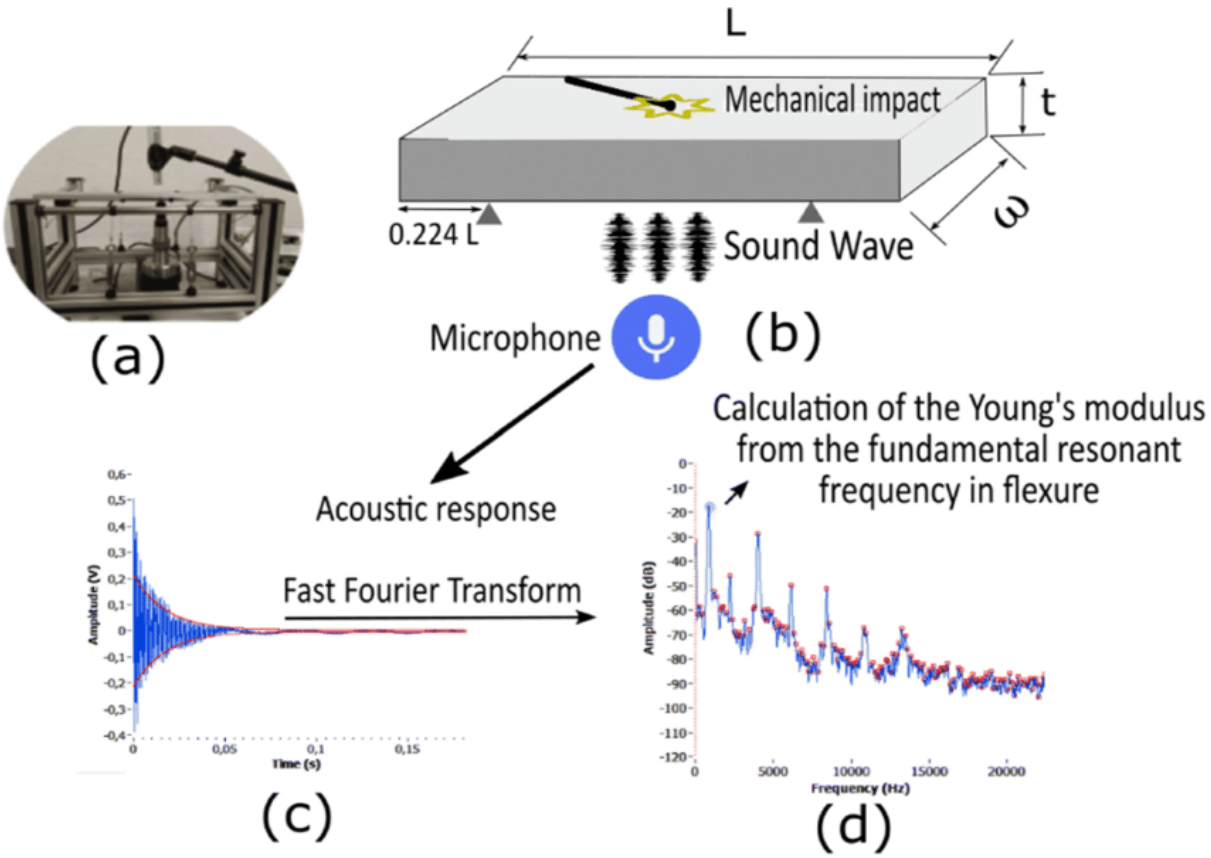


**Figure 3.9**: Schematic and procedure of the Impulse Excitation Technique (IET) used to determine the dynamic Young's modulus. (a) Experimental setup with specimen mounted in free–free condition. (b) Excitation by a light mechanical impact and recording of the acoustic response with a microphone. (c) Time-domain signal of the acoustic response. (d) Frequency-domain spectrum obtained via Fast Fourier Transform (FFT), from which the fundamental resonant frequency is identified and used to calculate Young's modulus.[xx]

For the aluminum material calibration, a cylindrical aluminum bar of 150 mm length (15 mm diameter) was used. This bar was suspended in a nearly free-free condition (using soft elastic strings to mimic free support). Using a small hammer, a mechanical impulse was applied to one end of the bar, and a microphone recorded the sound/vibration response. The resonant frequencies appear as peaks in the frequency spectrum of the recorded signal. We particularly monitored the first longitudinal mode. Using a commercial software (Buzz-o-Sonic), the dominant frequency of the ring was identified as 17,230 Hz for the 150 mm aluminum bar (**Figure 3.10**). This is in excellent agreement with classical theory: plugging into the formula for Young's modulus via the longitudinal frequency gives:

$$E = 4 \times \rho \times L^2 \times f^2 \quad \textbf{(7)}$$

where ρ is the material density, L is the specimen length, and f is the first longitudinal resonance frequency. By inserting the measured values (ρ = 2700 kg/m³, L = 0.150 m, f = 17,210 Hz) in (**7**), the modulus was obtained as E = 72.1 GPa.
This experimentally derived value (about 72.3 GPa) is slightly higher than the typical handbook value for the aluminum alloy (70 GPa). The difference may come from the alloy's temper condition or from small calibration effects in the measurement. For accuracy, this measured modulus was used in the finite element model to ensure that the simulated resonance frequencies matched the experimental results.

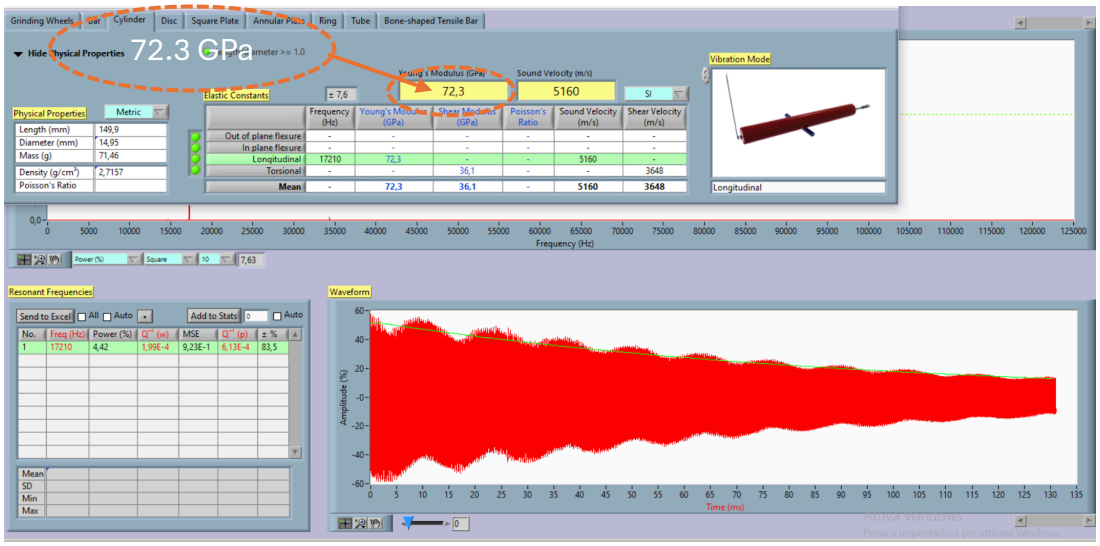


**Figure 3.10**: Longitudinal frequency peak from IET of the aluminum specimen. This figure shows the frequency spectrum obtained from the Buzz-o-Sonic software for the 150 mm aluminum bar, with a clear peak at 17.23 kHz corresponding to the first longitudinal resonance. The sharpness of the peak also gives an indication of the low damping in the material.

Having validated the aluminum properties, the next step was to perform a similar IET test on the bonded hybrid specimen. **Figure 3.11** shows a dominant peak at approximately 20.2 kHz, corresponding to the first longitudinal mode, which confirms that the specimen was successfully tuned to the target resonance frequency. A secondary peak appears near 41 kHz, which represents the second harmonic of the longitudinal vibration (where the bar vibrates with two half-waves along its length instead of one).

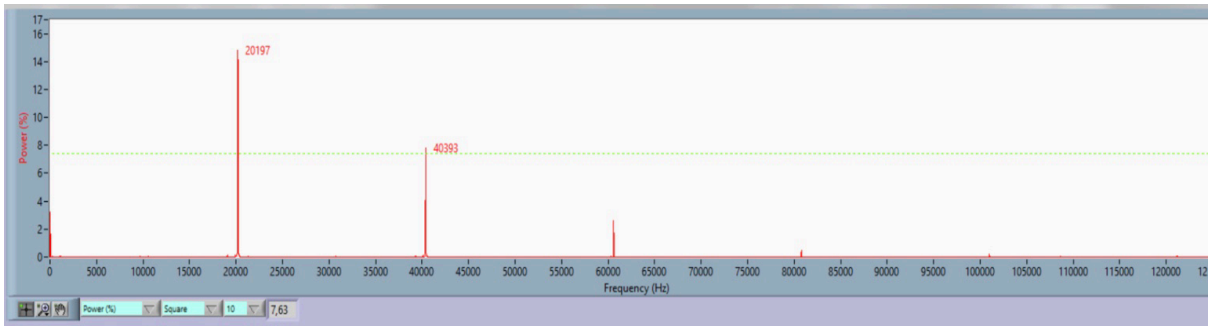


**Figure 3.11**: Resonance spectrum of the hybrid aluminum–CFRP specimen obtained from impulse excitation. The first longitudinal resonance is observed at 20,197 Hz, corresponding to the target ultrasonic frequency for VHCF testing. A second resonance peak is visible at 40,393 Hz, which corresponds to the second longitudinal mode. These results confirm that the specimen geometry was correctly tuned to achieve resonance close to 20 kHz.

In summary, IET provided experimental validation of the FE-predicted modal parameters. For the aluminum rod, it accurately yielded $E_{Al}$ and the frequency (we used a Buzz-o-Sonic software for automated determination of frequency). For the bonded joints, the IET results showed that the target resonance frequencies were reached with very small differences, within less than one percent, as well getting the right value of the elastic modulus out-of-plane of CFRP which is equal to 8.6 GPa.

### 3.6.2. Strain Gauge Calibration Method

In this section, using the hybrid specimen composed of 123 mm of the aluminum rod, a thin layer of adhesive (0.08 mm), and a CFRP rod (6.81 mm). A foil strain gauge (2 mm gauge length) was attached to the aluminum bar (**Figure 3.12**), but not at the interface, instead, it was placed in the middle of the aluminum section. The gauge was oriented along the axis of the rod so it could measure the axial strain during vibration. Before mounting the gauge, the aluminum surface was cleaned, lightly abraded, and degreased, and the same adhesive used in the hybrid specimen was used here to make sure the gauge would stay attached and give a stable signal. The reason for placing the gauge in the middle is that, in the first longitudinal vibration mode (around 20 kHz), the axial stress is highest in the middle of the specimen and close to zero at the ends. That means the signal at mid-span is mainly axial. During the calibration, the strain measured in that location on the aluminum was linked to the displacement amplitude at the free end of the specimen.

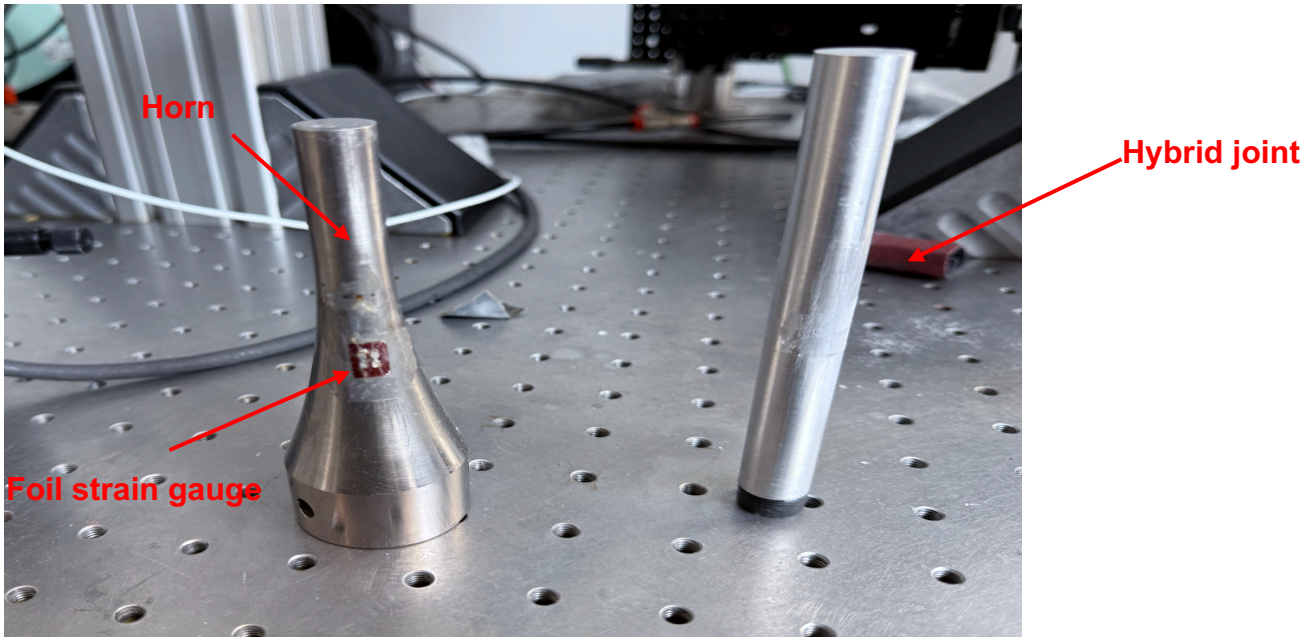


**Figure 3.12**: horn and hybrid rod preparation for the strain gauge test

The foil strain gauge indicated in **Figure 3.12** was temporarily bonded to the horn. Still, it was not instrumented in the present measurement and was not wired to any bridge configuration during this test, as illustrated in **Figure 3.13**.

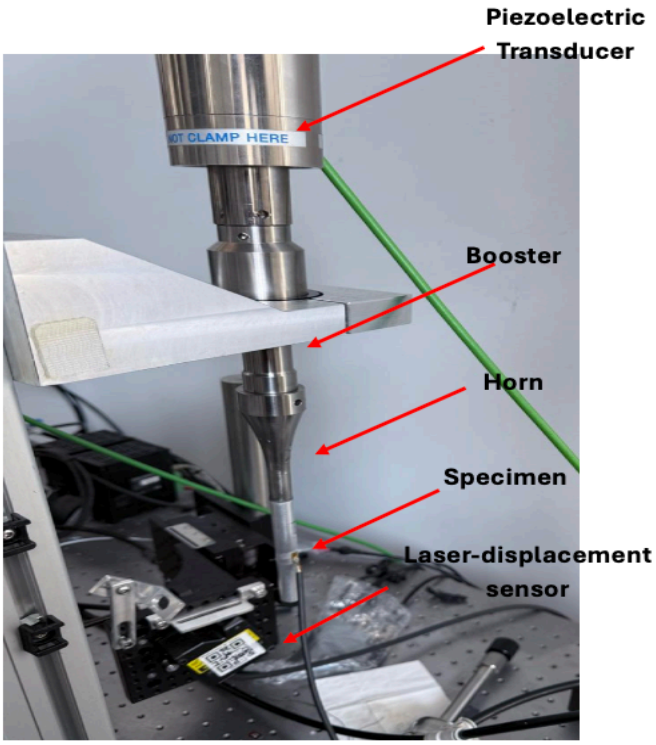


**Figure 3.13:** Experimental ultrasonic fatigue test setup for calibration. The aluminum rod–CFRP disk specimen is mounted in the 20 kHz ultrasonic resonant testing machine (transducer and booster assembly shown at top). The green cable is the lead

from the strain gauge bonded on the aluminum rod near the adhesive interface (the gauge itself is just beneath the clamping fixture). The strain gauge wiring is routed to a signal conditioner for dynamic strain measurement.

The hybrid specimen's aluminum bar was adhesively joined to the booster and horn of the piezoelectric transducer (**Figure 3.13**) so the full stack (transducer–booster–horn–specimen) acted as a half-wavelength resonator. A preliminary frequency sweep with the bonded specimen installed identified the operating resonance, with the instrument reporting a parallel resonance near 20,201 Hz and a series resonance near 20,202 Hz (**Figure 3.14**), confirming correct tuning at 20.2 kHz. At this frequency, a standing longitudinal wave forms: displacement is largest at the free CFRP end, while axial strain (and thus stress) peaks in the mid-span of the aluminum.
A foil strain gauge was connected in a quarter-bridge arrangement and bonded at the midpoint of the aluminum rod, allowing it to measure the strain in this region. The aluminum's axial stress was then calculated using Hooke's law.

$$\text{Hooke's law } (\sigma = E\,\varepsilon) \quad \textbf{(8)}$$

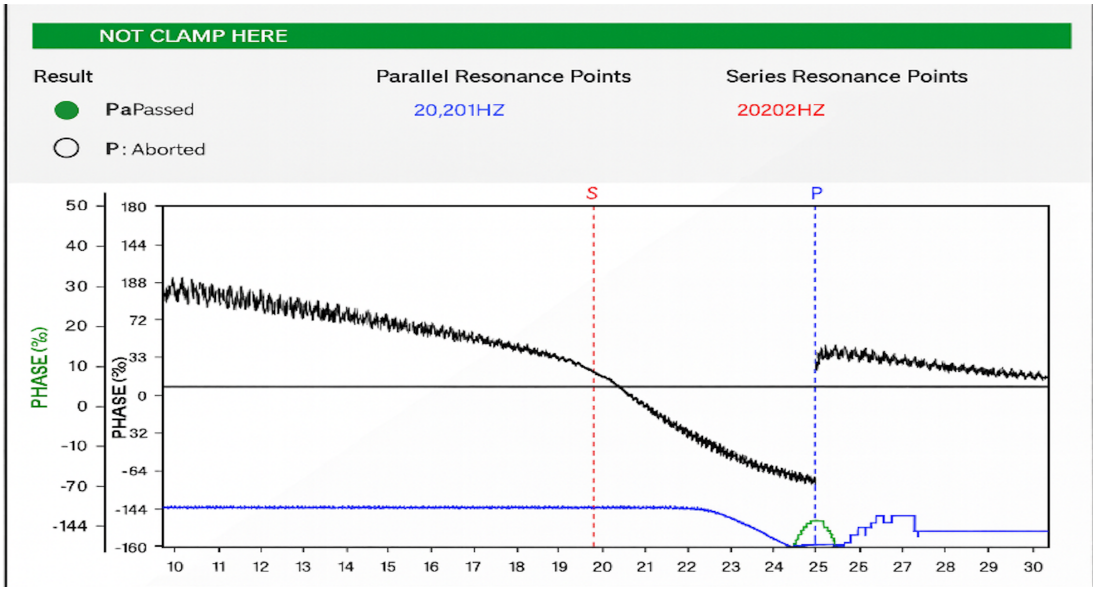


**Figure 3.14:** Ultrasonic resonance measurement of the hybrid specimen under free-free conditions.

**Calibration procedure:** To establish the relationship between displacement amplitude and stress, a series of low-amplitude excitation tests was carried out at gradually increasing drive levels. The ultrasonic transducer was driven with a sinusoidal voltage, starting from a very low amplitude (1.1 V) and then incrementally increasing the input to 1.5 V. For each drive setting, the displacement at the free-end was measured. In parallel, the strain gauge bridge output (an AC voltage at 20 kHz)

was monitored using a high-bandwidth data logger to capture strain amplitude. The dynamic strain at the gauge location was obtained from the bridge output (accounting for the bridge factor and amplifier gain) and then converted to stress via (**8**). Care was taken to keep these calibration excitations in the elastic regime and at modest amplitudes so that the gauge would not overheat or suffer fatigue damage during continuous 20 kHz operation. (Notably, at higher excitation levels, the gauge and adhesive can experience self-heating due to hysteresis and internal damping, which can slightly affect gauge resistance and readings. The calibration was limited to displacement amplitudes up to 15 μm to avoid any significant temperature rise, ensuring the strain measurements remained accurate). For each excitation level, a pair of readings, displacement amplitude $\delta$ and the corresponding stress $\sigma$ was obtained.

# **Chapter 4** : Results and Discussion

## 4.1. Changing out-of-plane elastic modulus $E_c$

In this analysis, the axial modulus of the CFRP block in the hybrid joint, $E_c$ (out-of-plane modulus) is changed while all other elastic properties of the CFRP, such as $E_a$ and $E_b$ were held constant (54 GPa). For the aluminum and adhesive nothing was changed. The main result is that changing $E_c$ slightly affected the global resonance of the specimen. The first bending modes (Modes 1 and 2) increased only slightly, from about 18.989 kHz at $E_c$ = 5 GPa to 19.058 kHz at $E_c$ = 20 GPa, which is less than a 0.4% change. The main axial (longitudinal) mode shifted from about 20.037 kHz at $E_c$ = 5 GPa to 20.071 kHz at $E_c$ = 20 GPa. That is a total difference of roughly 34 Hz, which is below 0.2% of total 20 KHz. This shows that the dynamic response of the whole specimen is dominated by the long aluminum bar (about 72 GPa axial modulus) rather than by the short CFRP insert. That realistic scatter in the CFRP's out-of-plane stiffness will not force any serious re-tuning of the machine to stay near 20 kHz.

| $E_c$ | 5 GPa | 10 GPa | 15 GPa | 20 GPa |
|---|---|---|---|---|
| **Mode 1** | 18.989 | 19.0358 | 19.050 | 19.058 |
| **Mode 2** | 18.989 | 19.0358 | 19.050 | 19.058 |
| **Mode 3 (axial)** | 20.037 | 20.060 | 20.0675 | 20.071 |
| $\frac{\sigma}{\delta} = \frac{SIGMA_x \text{ at the end}}{DISPLACEMENT \text{ at the end}}$ | 11.71 | 10.79 | 10.539 | 10.96 |

**Table 4:** Effect of changing the out-of-plane Elastic Modulus on frequencies and $\frac{\sigma}{\delta}$

Tracking also how the stress–displacement ratio ($\sigma/\delta$) reacted to this $E_c$ change. Here $\delta$ is the axial displacement at the free end of the specimen and $\sigma$ is the corresponding axial stress measured in the FE model in that same region (where the CFRP is located). So $\sigma/\delta$ tells us how much axial stress we get in the joint region per unit tip displacement. The trend was not purely monotonic. When $E_c$ = 5 GPa, $\sigma/\delta$ was around 11.71 MPa per unit displacement. As $E_c$ increased to 10-15 GPa, $\sigma/\delta$ dropped into the 10.5-10.8 MPa range. When $E_c$ was pushed to 20 GPa, $\sigma/\delta$ reduced slightly again to about 10.96 MPa per unit displacement. This behavior makes physical sense when considering what the adhesive layer is doing at the free end. When the composite is very soft through its thickness (low $E_c$), the aluminum tries to oscillate at high stiffness, and the CFRP tries to move like a softer body. The thin adhesive layer at the interface (approximately 0.08 mm thick) is the only thing forcing the CFRP end to follow the aluminum's motion. That mismatch creates relatively high stress transfer per unit displacement at the free end, which is why $\sigma/\delta$ is high at 5 GPa. As the CFRP becomes stiffer in the loading direction (higher $E_c$), it follows the aluminum more

compatibly, so the interface is fighting less, and the stress per unit displacement drops. When $E_c$ increased, approaching 20 GPa, the CFRP specimen starts acting more like a rigid plug, and local stress near the bonded region builds again, so $\sigma/\delta$ increased slightly.

## 4.2. Effect of Adhesive Thickness on Frequency and Stiffness

One of the key investigations was how the adhesive layer thickness (bondline thickness) affects the specimen's natural frequencies and the stress transfer in order to choose the right thickness for our studies. Using the FE model, computing the modal frequencies for several adhesive thickness values while keeping other parameters constant (aluminum 125 mm, composite 6.81 mm, adhesive modulus 3 GPa). The results clearly showed a trend of decreasing natural frequencies with increasing adhesive thickness. This is expected: a thicker adhesive acts like a more compliant spring between the aluminum and composite, reducing the overall stiffness of the assembly.

For instance, in the simulation for the carbon rod (having more than 1 layer, notifying the difference will be easier and the study will be more accurate):

- With a very thin adhesive of 0.05 mm, the first bending mode was 16.38 kHz, the longitudinal mode (axial) was 17.42 kHz, and the first torsional mode was 19.81 kHz.
- Increasing the adhesive to 0.15 mm (three times thicker) dropped those frequencies to roughly 16.07 kHz (bending), 17.12 kHz (longitudinal), and 19.40 kHz (torsion).

The longitudinal mode (axial) showed only a modest decrease (1.7% drop from 17.42 to 17.12 kHz) over that large thickness change. Bending and torsional modes dropped a bit more in percentage terms (bending 1.9%, torsion 2.1%). This indicates that all modes become softer (lower frequency) with a thicker adhesive, but the effect is more pronounced for bending and torsional modes. Bending and torsion engage shear and peel deformations at the interface more, so they are more sensitive to bond thickness. The axial mode primarily engages the adhesive in direct tension/compression along the thickness, which for thin layers is very stiff. Making it thicker adds some compliance, but since the adhesive's in-plane area is large and it's loaded in a relatively stiff way (through-thickness compression), the effect is smaller.

Beyond just the frequencies, the stress–displacement ratio ($\sigma/\delta$) was found to degrade with thicker adhesives (**Figure 4.1**). In quantitative terms, at 0.05 mm thickness the ratio was around 9.92 MPa per mm, whereas at 0.15 mm it fell to about 8.29 MPa per mm. This roughly 17% decline in $\sigma/\delta$ means that for the same vibration amplitude (displacement), the stress transmitted through the adhesive is lower when the adhesive is thicker. Essentially, a thicker adhesive absorbs more deformation, so the composite is loaded with less stress. This confirms the idea that a thicker layer is less efficient in transferring stress.

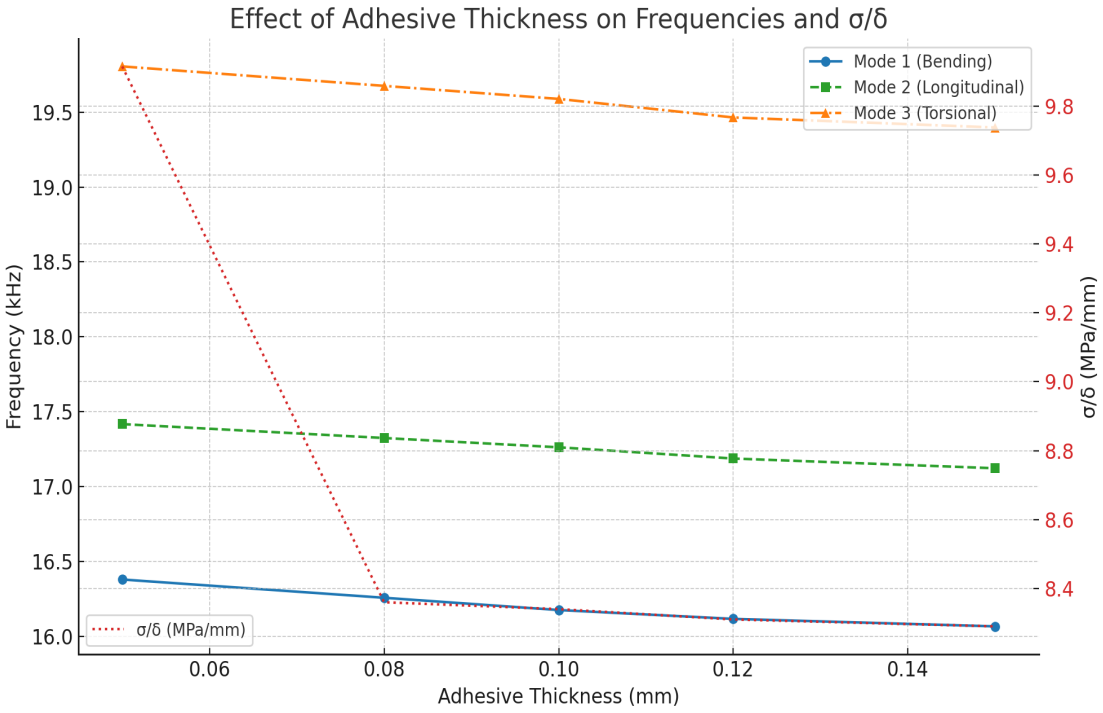


**Figure 4.1:** The effect of adhesive thickness on stress/displacement ratio $\frac{\sigma}{\delta}$ and on frequencies

The FE analysis also provided insight into the mode shape details: with thicker adhesive, there was slightly more bending of the adhesive layer in bending modes and more shear deformation in torsion. But in all cases, the adhesive remained intact (not broken).

The interpretation of these results is that a thicker adhesive acts like a soft cushion or buffer. It lowers the global stiffness, which is directly reflected in lower natural frequencies for all vibration modes. Torsional and bending modes are especially sensitive because they put the adhesive in shear and peel, where a thicker layer lowers stiffness. The axial mode's slight sensitivity (small frequency drop) suggests that even in axial loading, the thicker adhesive slightly reduces axial stiffness of the joint, making the system a bit more compliant longitudinally. The consistent but small decrease in $\sigma$ /$\delta$ With thickness, there is a gradual loss of stress transfer efficiency. Even if the effect on axial frequency is subtle, the adhesive is doing more deformation work rather than passing the load to the composite.

From a design perspective, these findings highlight that thin adhesive layers (in the range of 0.05–0.08 mm) are preferable for maintaining high stiffness and resonant frequency. If one's goal is to maximize the frequency (hitting higher target or keeping the structure stiff), keeping the bondline thin is beneficial. Additionally, for a given excitation amplitude, a thin layer will experience higher stress (which, for fatigue testing, might be desired to induce failure faster). Conversely, increasing adhesive thickness beyond 0.1 mm significantly reduces dynamic performance: in this case going to 0.15 mm showed notable drops in performance. Thus, practically, one should

control the adhesive thickness tightly when fabricating such specimens. Manufacturing variances in bondline thickness can lead to measurable differences in resonant frequency and may require retuning of the system.
It should be noted that extremely thin layers (below 0.05 mm) were not studied but could pose other issues like incomplete wetting or higher stress concentrations (not captured in this simple model). There is likely an optimal minimum thickness that provides a continuous bond without voids, but still as stiff as possible.

## 4.3. Effect of Adhesive Modulus on Frequency and Stress Transfer

Another important parametric study was varying the adhesive's Young's modulus to see how a softer or stiffer adhesive material would influence the specimen's behavior. We examined adhesive modulus from 1000 MPa (1 GPa) up to 5000 MPa (5 GPa), which goes from a flexible adhesive to a very stiff one. The bondline thickness in this study was held constant (around 0.08 mm) to isolate the effect of material stiffness.
The simulation results showed that increasing the adhesive modulus raised the natural frequencies slightly, but with diminishing returns at higher modulus. Specifically, as the $\mathrm{E_{adhesive}}$ went from 1 GPa to 2 GPa, seeing a small increase in frequencies. For example, one bending mode frequency went from 18.77 kHz to 19.04 kHz between 1 and 2 GPa, and then beyond 2 GPa it more or less plateaued around 19.05 kHz. Essentially, above about 2–3 GPa, making the adhesive even stiffer did not significantly change frequencies (the structure had reached a point where the adhesive is stiff enough that the joint behaves almost as if it were rigidly bonded). In fact, the modes became nearly insensitive to further increases in adhesive stiffness (**Figure 4.2**).

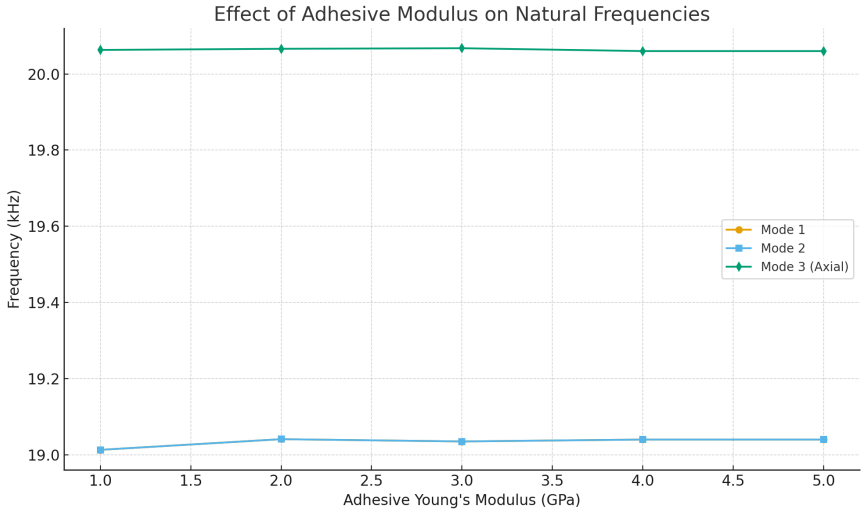


**Figure 4.2:** This graph shows the effect of adhesive modulus on the frequencies of different modes

The axial mode frequency was almost flat across this range: at 1 GPa adhesive, the axial (longitudinal) mode was 20.06 kHz. It increased to 20.067 kHz at 2 GPa, and then interestingly slightly dropped back to 20.06 kHz at 5 GPa. This tiny variation (<0.05%) indicates that the axial mode is practically governed by the base materials (aluminum/composite) and geometry, with adhesive stiffness only mattering when it's extremely low. The initial slight increase and then drop might be an artifact or due to interplay with other modes, but effectively, the axial frequency is very low in sensitivity to adhesive modulus. This makes sense: in axial loading, even a relatively soft adhesive (1 GPa) in a 0.08 mm layer is still much stiffer axially than the equivalent compliance of the metal parts (because the cross-sectional area is large). Only if the adhesive were extremely soft it will significantly elongate under the same force and reduce axial stiffness noticeably.

The stress/displacement ratio $\sigma/\delta$ (**Figure 4.3**), showed a more interesting trend with adhesive modulus. At 1 GPa, $\sigma/\delta$ was relatively high (the simulation gave about 10.59 MPa/mm at 1 GPa), it then dropped slightly to 10.54 MPa/mm at 2 GPa, but as modulus increased, further $\sigma/\delta$ increase sharply, reaching about 10.79–10.80 MPa/mm at 3 GPa and plateauing around there. By 5 GPa, a slight drop was observed in $\sigma/\delta$. These numbers suggest that there is a critical stiffness around 2–3 GPa where the adhesive becomes effective at transferring load. Below that, the adhesive is so compliant that increasing it from 1 to 2 GPa actually made $\sigma/\delta$ drop a tiny bit – this is somewhat counterintuitive at first glance, but it could be due to the mode shape normalization or how stress concentrates. However, from 2 GPa to 3–4 GPa, the adhesive's ability to carry load improves, raising $\sigma/\delta$. Beyond 4 GPa, further stiffening doesn't help and at 5 GPa, noticing a minor decline, possibly due to stress concentrating at the ends of the adhesive (a very stiff adhesive might approach a hard inclusion, causing local stress concentration that slightly reduces the average $\sigma/\delta$ efficiency).

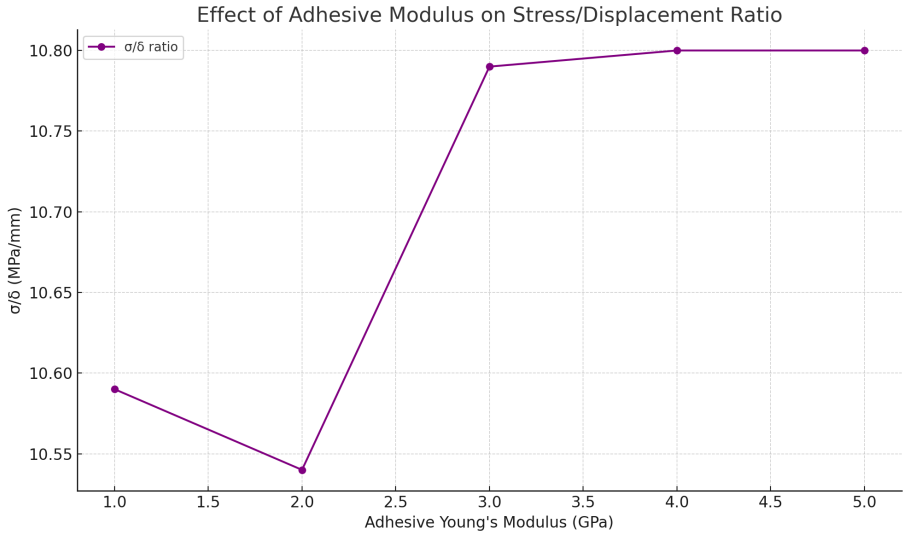


**Figure 4.3**: The effect of adhesive modulus on stress/displacement ratio $\frac{\sigma}{\delta}$

In plain terms, making the adhesive stiffer improves the joint's load transfer up to a point where the adhesive does not become too rubbery. But if the adhesive is already quite stiff (a few GPa), making it even stiffer contributes to a little benefit in terms of dynamic response. The system is largely as stiff as it can get. And if one were to approach the stiffness of aluminum (72 GPa), other issues might come in such as brittleness or, as mentioned, local stresses.

**Interpretation**: These findings can be interpreted as evidence of an optimal adhesive stiffness. When the adhesive is too soft (1 GPa or below), the joint is floppy – frequencies are a bit lower and, importantly, the stresses for a given displacement are lower (meaning energy is going into deforming the adhesive, not into generating high stress). As the stiffness of the adhesive increases, the joint becomes more monolithic (acts as a 1 single rod) and better at carrying load ($\sigma$ /$\delta$ increases), which is beneficial for strength. But once the adhesive stiffness exceeds a few GPa, the joint is already quite stiff and further increases yield diminishing returns.

From a design viewpoint, using a standard high-strength epoxy (which usually has E in the 2–4 GPa range) is ideal – it gives optimal frequency and load transfer. Using an even stiffer adhesive (if one existed, say a very highly filled epoxy or a metal solder) wouldn't significantly boost performance and might cause other problems. Using a much softer adhesive (like adhesive with $\mathrm{E}_{\mathrm{adhesive}}$ equal to 0.1–0.5 GPa) would degrade the resonant frequency and require much more input to get the same stress, so it's not suitable for ultrasonic applications where stiffness matters for resonance.

In summary, the adhesive modulus has a strong influence on stress transfer, but only up to a point. The optimum lies around 2–3 GPa, which explains why structural epoxies are commonly used in hybrid joints for aerospace and automotive applications. Softer adhesives would degrade performance and may fail, while stiffer adhesives do not provide major benefits and may increase stress concentrations. The combination of numerical analysis and experimental verification shows that our joint design falls within

the effective range, with the chosen adhesive providing a reasonable compromise between stiffness, bonding quality, and practical handling.

## 4.4. Strain gauge calibration results

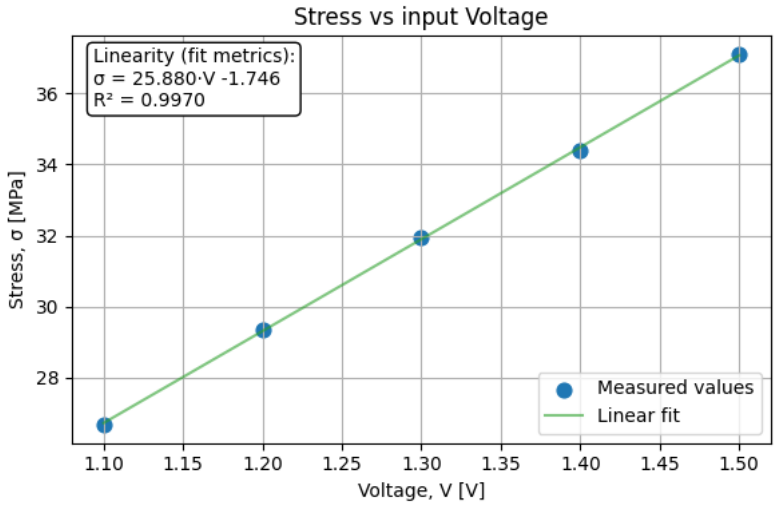


**Figure 4.4:** Calibration curve showing the linear relationship between input voltage and corresponding stress in the aluminum–CFRP hybrid specimen.

During the experimental phase, measuring the strain in the middle of the aluminum bar of the hybrid aluminum–adhesive–CFRP specimen. The goal of this test was to establish a precise relation between the displacement at free-end and the axial stress in the specimen, and compare these results to FE. Once it is validated, establishing a relation between stress in the middle of the adhesive and displacement will be possible and valuable. The input voltage was increased from 1.1 V to 1.5 V (**Figure 4.4**), generating stable longitudinal vibrations at the free end with amplitudes ranging from 11 μm to 15 μm (**Figure 4.5**). The strain gauge readings increased linearly with displacement, leading to the calibration equation:

$$\sigma = 2.55\ \delta - 1.343 \quad \textbf{(9)}$$

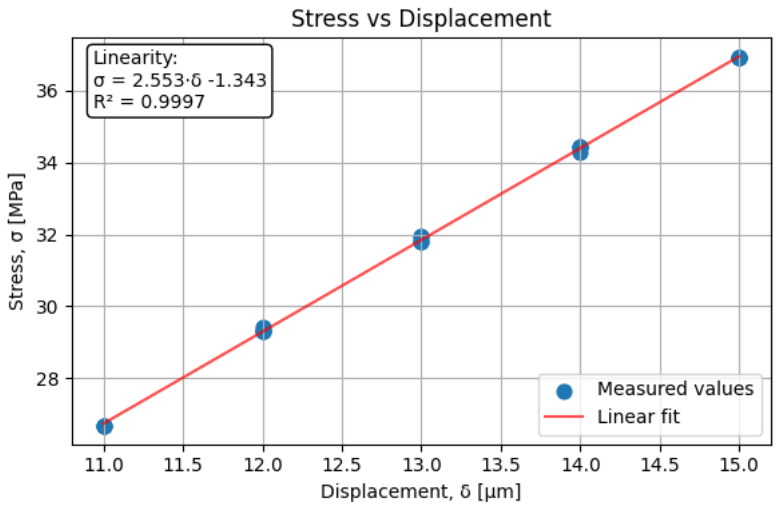


**Figure 4.5:** Calibration curve showing the linear relationship between input displacement amplitude and corresponding stress in the aluminum–CFRP hybrid specimen.

where σ is the aluminum stress in MPa and δ is the displacement in micrometers at the free-end. The linearity was excellent ($R^2$ = 0.9997), confirming highly consistent elastic behavior.

The measurements also showed an excellent linear link between the input voltage and the axial stress in the aluminum (**Figure 4.5).** Over tested range (1.1 to 1.5 V), stress increased from 26.8 to 36.9 MPa, leading to the calibration equation:

$$\sigma = 25.497\ V_{in} - 1.746 \quad \textbf{(10)}$$

The linearity was excellent ($R^2$ = 0.9997) for these two measurements.

The finite element (FE) simulation in LS-DYNA, performed at the first longitudinal mode (20 kHz), predicted a normalized stress of 17,170 at the gauge location (in the middle of aluminum part) and 1,754 in the middle of the adhesive layer (see **Figure 4.6**) extracted from LS-DYNA.

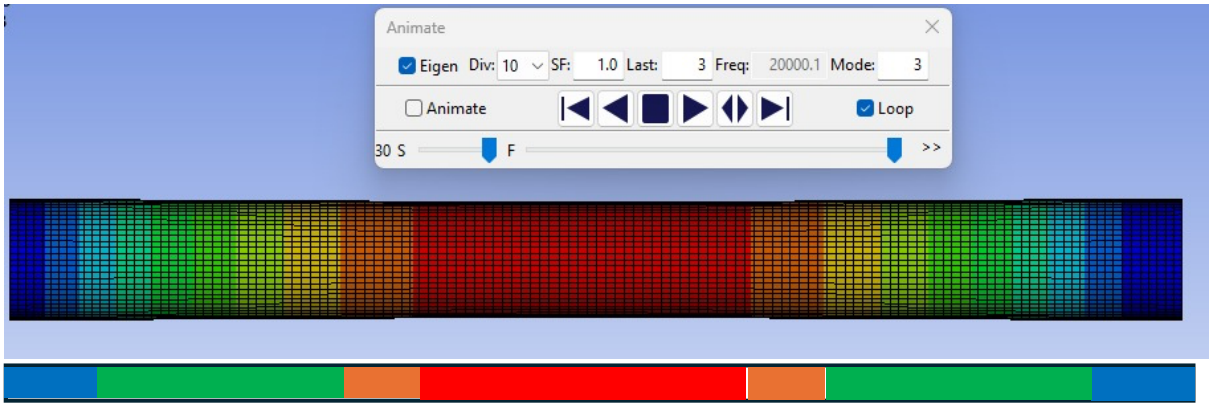


MPa 1.2551e+02 5.352e+3 15.816e+3 1.7170e+04 15.816e+3 5.352e+3 1.2551e+02

**Figure 4.6:** The axial stress in the x direction for the hybrid specimen giving the maximum stress in the middle with a value of 17,170 MPa vs 125.51 at the free-end while holding it at 20 KHz.

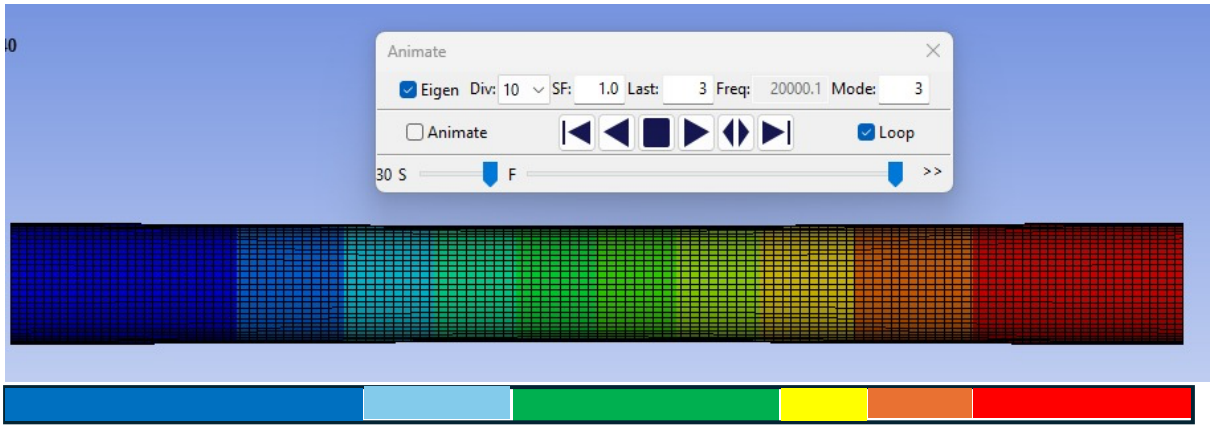


mm -6.274 -2.386 1.502 5.390 6.029 6.686

**Figure 4.7:** The axial displacement in the x direction for the hybrid specimen giving the maximum displacement in the end with a value 6.686 mm

**FE:** The FE at the gauge location gave an aluminum stress of 17,170 with a free-end displacement of 6.686 mm. These two numbers are on the same FE scale:

$$(\sigma/\delta)_{\mathrm{FE}} = \frac{17170}{6.686\ \mathrm{mm}} = 2.568\ \mathrm{MPa/\mu m} \quad \textbf{(11)}$$

**Experimental calibration:** the strain-gauge/laser test gave **(9)**
$(\sigma/\delta)_{\mathrm{EXPERIMENTAL}}$ =2.55 $\delta$ -1.343 MPa/μm.
Knowing $(\sigma/\delta)_{\mathrm{FE}}$ gave the possibility to estimate the stress for each displacement value.

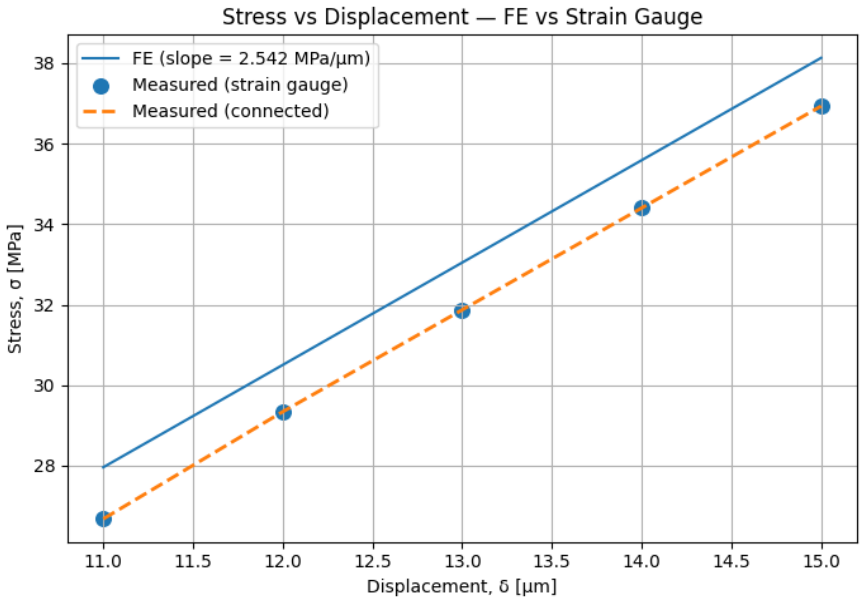


**Figure 4.8:** Comparison between $\sigma_{FE}$ *and* $\sigma_{Calibration}$.

From the FE simulation, getting $\sigma_{adhesive}$=1,704 in the middle of the adhesive layer and $\sigma_{aluminum}$= 17,170 in the middle of the aluminum bar, so the ratio k =$\frac{1,704}{17,170}$ =0.0976 (9.76 %).
Combining (**9**) with this ratio to get the adhesive stress in function of displacement that can be directly usable in tests:

$$\sigma_{\text{adhesive}} = k \times (2.55\,\delta - 1.343) = 0.0976 \times (2.55\,\delta - 1.343) \qquad \textbf{(12)}$$

The consistent ratio between adhesive and aluminum stresses (9.76%) confirms that the adhesive layer carries the expected fraction of the load under axial vibration. This ratio is physically realistic and arises from the constrained compression state of the thin 0.08 mm adhesive bondline between materials of different stiffness.
Finally, **Table 5** shows the difference of stresses in the middle of aluminum bar ($\sigma_{\text{Calibration}}$ and $\sigma_{\text{FE}}$) and $\sigma_{\text{adhesive}}$ in the middle of the adhesive layer.

| Displacement δ [μm] | Stress $\sigma_{\text{FE}}$ [MPa] | Stress $\sigma_{\text{Calibration}}$ [MPa] | Error | Stress $\sigma_{\text{adhesive}}$ [MPa] |
|---|---|---|---|---|
| 11 | 28.248 | 26.68 | 1.5 % | 2.768 |
| 12 | 30.816 | 29.44 | 1.3 % | 2.885 |
| 13 | 33.384 | 32.12 | 1.26% | 3.1477 |
| 14 | 35.952 | 34.43 | 1.5% | 3.374 |
| 15 | 38.52 | 37.15 | 1.37% | 3.6407 |

**Table 5:** Comparison between $\sigma_{\text{FE}}$ and $\sigma_{\text{Calibration}}$ and $\sigma_{\text{adhesive}}$.

# **Chapter 5** : Conclusions

This work developed and validated a hybrid aluminum–adhesive–CFRP resonant specimen for ultrasonic (20 kHz) testing. Using LS-DYNA modal analysis, impulse excitation (IET), and strain-gauge calibration, the study established how adhesive thickness and modulus influence resonance and stress transfer, and how uncertainty in the CFRP out-of-plane modulus $E_c$ affects global dynamics, and a simple stress–displacement control law that turns machine tip motion or voltage into a reliable estimate of axial stress at the joint and in the adhesive layer as well. The main conclusions are grouped below.

## 5.1. Frequency targeting and model credibility

For the final geometry (125 mm Al + 6.8 mm CFRP + 0.08 mm adhesive), the FE-predicted first longitudinal mode sits essentially at 20 kHz. The measured response is within a few tens of hertz. This agreement indicates that (a) a linear, undamped modal model is sufficient for frequency placement, and (b) the long aluminum part dominates the global inertia–stiffness balance at 20 kHz. These findings are consistent with standard IET practice for metals and bars[xxi] and with the observation that global resonances in slender, axially vibrating rods are governed by the stiffer, longer segment.

## 5.2. Adhesive thickness

When the bondline increased from 0.05 to 0.15 mm, all modes dropped in frequency (global softening) and the stress-per-displacement ratio fell by 17 % (9.92 → 8.29 MPa/mm in the FE normalization used). Bending and torsional modes were more sensitive than the axial mode because thicker bondlines reduce shear stiffness at the interface, which those modes rely on. This matches classic bonded-joint theory: increasing thickness lowers lap/peel stiffness and tends to raise local peel stresses near the edges[xxii]. For ultrasonic work, thin, uniform bondlines (0.05–0.08 mm) are preferred: they preserve frequency and improve transfer efficiency.

## 5.3. Adhesive modulus

Changing the adhesive modulus from 1 to 5 GPa produced modest frequency changes that saturated once $E_{adhesive}$ = 2–3 GPa. The stress/displacement metric improved from soft to semi-rigid adhesives and then flattened, with a slight decline at 5 GPa. Once the bondline reaches a moderate stiffness, the axial response of the joint is

controlled by the adherends (carbon and aluminum). An increasing in the adhesive modulus offers little benefit to the global behavior and can amplify edge stresses. This agrees with reports on stiffness and rate effects in structural epoxies. For the present geometry and frequency, an adhesive in the 2–4 GPa range is therefore a practical optimum.

## 5.4. Strain-gauge calibration

By bonding a foil strain gauge in the middle of the specimen, make it possible getting the axial stress in the aluminum by driving whether an input displacement or an input voltage, and using the FE simulation gives the possibility to validate results and make a relation between stress in the middle of aluminum and in the middle of the adhesive. Knowing the stress in the adhesive changes how the whole experiment is interpreted. It gave the possibility to program the 20 KHz ultrasonic fatigue rig by target stress in the adhesive, hitting meaningful VHCF ranges without wasting time on under-loads or risking sudden failures from overloads. On the modeling side, adhesive-stress data give the possibility to calibrate S–N models against the quantity that governs damage, which tightens correlation between FE and tests and makes life predictions more trustworthy.

During long runs, tracking adhesive stress at a fixed displacement and the stress-to-displacement ratio or the resonant frequency drift acts as an early warning for stiffness loss and micro-cracking.

## 5.5. Limitations and scope

The modal analysis was linear and undamped. Damping and thermo-viscoelastic effects were not quantified here. Edge singularities (adhesive ends) were not resolved with fillets/tapers or sub-modeling. Calibration was done at modest amplitudes, so self-heating and amplitude-dependent damping were not mapped. These choices were deliberate to first secure a clean resonant baseline before moving to VHCF testing and damage modeling.

## 5.6. Industrial implications

For bonded hybrid parts operating near ultrasonic frequencies (sensors, horns, lightweight connectors), three practical rules emerge:

First, holding the bondline tightly in the 0.05- 0.08 mm range: thin, uniform adhesive layers keep the joint stiff and improve stress transfer (higher $\sigma/\delta$).

Second, using a semi-rigid epoxy ($E_{adhesive}$ = 2- 4 GPa): This sits in the spot where the joint behaves nearly monolithic without introducing edge-peel penalties that come with ultra-stiff bonds.

Third, don’t over-worry about CFRP out-of-plane modulus scatter: reasonable variation in $E_c$ shifts the 20 kHz resonance only marginally, so frequency retuning is minimal. Instrumenting the metal side with a foil gauge and establishing a simple $\delta$ to $\sigma$ calibration to run tests (and service checks) in stress control rather than displacement control. Together, these practices give predictable resonance, cleaner energy transfer, and easier quality control (fully consistent with classic bonded-joint design guidance and modern adhesive reviews)[xxiii].

# **Chapter 6** : Future Work

The program shifts from dynamic readiness to fatigue evidence. Below is a prioritized plan that fills knowledge gaps while providing maximum payoff per unit effort.

## 6.1. S–N data at 20 kHz with health monitoring

To build the VHCF evidence base, running a compact S–N program at nominal adhesive stresses of 12, 15, 20, 25, and 30 MPa, using the calibrated stress–displacement law **(9)** to set the machine amplitude. Logging both failures and run-outs in the $10^8 - 10^9$ cycle range. Controlling temperature by embedding a small thermocouple close to the bondline (or taking periodic IR images), capping the adhesive temperature near 40 °C, and using duty cycles or a directed air jet if heating is observed, since high-frequency loading can stiffen viscoelastically and generate heat that would confound life estimates. In parallel, tracking two health indicators at a fixed commanded $\delta$: the resonant-frequency drift and the gauge-based $\sigma/\delta$. A gradual frequency drop or a systematic change in $\sigma/\delta$ is a sensitive early sign of stiffness loss and incipient damage, allowing to flag crack initiation without interrupting the test.

## 6.2. Voltage to displacement mapping

In the lab we typically set drive voltage, then verify free-end displacement with the laser. We'll formalize that by sweeping near resonance, recording $\delta$ (V), and fitting a simple line over the safe range. Combining $\delta$ (V) with the validated $\sigma_{\mathrm{aluminum}}(\delta)$ gives a direct $\sigma_{\mathrm{aluminum}}(\mathrm{V})$, and via k, getting $\sigma_{\mathrm{adhesive}}(\mathrm{V})$. A small check catches drift from temperature or fixture changes. Then publishing a quick-reference table (e.g., 1.1 V → 11 μm → 27 MPa Aluminum, 1.5 V → 15 μm → 37 MPa) so operators can hit a target stress using either displacement or voltage with the same confidence.

## 6.3. Specimen vs full-stack workflow

Keeping two complementary FE models. The specimen-only model (free–free, fast solves) is the main indicator of how trends shift (changing bondline thickness, adhesive modulus, or $\mathrm{E_c}$) and for extracting the stress ratio k=$\sigma_{\mathrm{adhesive}}/\sigma_{\mathrm{aluminum}}$. The full-stack model (horn + booster + specimen) is the reality bridge: it converts tip motion into the mid-bar stress under the true boundary conditions. Both will share the same material set and mesh discipline and doing periodic cross-checks (after any hardware change), so the specimen-only trends remain trustworthy while the full-stack model keeps us tied to what the machine actually delivers. This split keeps iterations fast without losing fidelity where it matters.

## 6.4. Adhesive stress law for test planning

With the reconciled slope and the FE stress ratio, publishing a one-line planning rule in **(12).**

Giving also bounds are derived from the sensitivity map (e.g., k = 0.10), so users know the expected spread due to build tolerances. A quick example: to reach $\sigma_{\text{adhesive}} = 3\text{MPa}$ with k = 0.10, results from $\sigma_{\text{aluminum}} = 30\ \text{MPa}$, i.e., $\delta = \frac{30+1.296}{2.55}$ = 12.3 µm. Pairing this with a simple temperature guardrail (keeping the bondline under 40 °C) and a note on duty cycles, so chosen amplitudes are both mechanically correct and thermally safe. This provides a clear, low-overhead method for programming stress for VHCF runs, comparing specimens fairly, and documenting settings.

## 6.5. Environmental and aging sensitivity

Humidity/temperature conditioning: Conditioning a subset of specimens before testing (for example, 50 samples, 70 % RH, 7 days) and repeat the standard resonance $\sigma/\delta$ calibration and a short fatigue step test. Recording changes in resonant frequency, Q, and calibrated stress for a fixed displacement. Adhesive stiffness and damping are known to shift with moisture uptake and temperature. Quantifying the frequency drop, Q reduction, and any rise in self-heating under identical drive builds a direct link to service conditions. Reporting the reversible (thermal) vs. irreversible (moisture/aging) components so test settings can be adjusted in advance for field-relevant environments.

Sub-endurance dwell tests: Running long on-resonance dwells at stresses below the estimated fatigue limit while tracking three simple indicators: resonant frequency, $\sigma/\delta$ at a fixed $\delta$, and temperature. The objective is to detect slow property drift (viscoelastic aging, moisture redistribution) that occurs without crack growth. Separating this drift from true damage makes later life data cleaner and improves model calibration.

[i] C. Bathias and P. C. Paris, *Gigacycle Fatigue in Mechanical Practice*. CRC Press, 2004.

[ii] A. Sonsino, "Course of SN-curves especially in the high-cycle fatigue regime," *International Journal of Fatigue*, vol. 29, no. 12, pp. 2246–2258, 2007.

[iii] C. Bathias, "There is no infinite fatigue life in metallic materials," *Fatigue & Fracture of Engineering Materials & Structures*, vol. 22, no. 7, pp. 559–565, 1999.

[iv] T. Sakai, "Historical review and future prospect for researches on very high cycle fatigue of metallic materials," *Fatigue & Fracture of Engineering Materials & Structures*, 2023.

[v] L.-L. Zhang, Y.-D. Li, and X.-Y. Liu, "On the formation mechanisms of fine granular area (FGA) in the VHCF regime," *International Journal of Fatigue*, vol. 92, pp. 434–446, 2016.

[vi] Li, R., Zhang, W., Paolino, D. S., & Peng, Y. (2025). *CALC−ΔKth: Automatic Assessment of the Stress Intensity Factor Threshold From VHCF Fracture Surfaces With Optically Dark Area.* Fatigue & Fracture of Engineering Materials & Structures.

[vii] Adams, R.D. and Wake, W.C., 1986. *Structural Adhesive Joints in Engineering*. London: Chapman & Hall.

[viii] Banea, M.D. and da Silva, L.F.M., 2009. Adhesively bonded joints in composite materials: an overview. *Proceedings of the Institution of Mechanical Engineers, Part L: Journal of Materials: Design and Applications*, 223(1), pp.1–18.

[ix] Stanzl-Tschegg, S.E., 2014. Very high cycle fatigue testing. *International Materials Reviews*, 59(7), pp.455–477.

[x] Vitaliy Kazymyrovych, "Very high cycle fatigue of engineering materials (A literature review)," Karlstad University Studies 2009:22, Karlstad University, Faculty of Technology and Science, Materials Engineering, 2009. ISBN 978-91-7063-246-4.

[xi] Pederbelli, M., *et al.*, 2023. Frequency effects in VHCF of structural epoxy adhesive butt joints at 20 kHz.

[xii] Pederbelli, M., *et al.*, 2023. Frequency effects in VHCF of structural epoxy adhesive butt joints at 20 kHz.

[xiii] Stanzl-Tschegg, S.E., 2014. Very high cycle fatigue testing. *International Materials Reviews*, 59(7), 455–477.

[xiv] A. Tridello, D. S. Paolino, L. Goglio, G. Chiandussi, and M. Rossetto, "Ultrasonic Very High Cycle Fatigue (VHCF) tests on a cyanoacrylate and on a high strength epoxy adhesive," in *Proceedings of the 12th European Adhesion Conference and 4th Luso-Brazilian Conference on Adhesion and Adhesives*, Lisbon, Portugal, Sept. 5–7, 2018, pp. 265–267.

[xv] D. Pederbelli, D. S. Paolino, A. Tridello, and L. Goglio, "An innovative methodology for the efficient numerical simulation of adhesive joints subjected to ultrasonic very-high-cycle fatigue tests," in *Proceedings of the 6th International Conference on Structural Adhesive Bonding (AB 2021)*, Porto, Portugal, July 8–9, 2021.

[xvi] Bathias, C., 1999. There is no infinite fatigue life in metallic materials. *Fatigue & Fracture of Engineering Materials & Structures*, 22(7), pp.559–565.

[xvii] Tridello, A., Paolino, D. S., Goglio, L., Chiandussi, G., and Rossetto, M., "Ultrasonic Very High Cycle Fatigue (VHCF) tests on a cyanoacrylate and on a high strength epoxy adhesive," Proc. 12th European Adhesion Conference and 4th Luso-Brazilian Conference on Adhesion and Adhesives, Lisbon, Portugal, 5–7 Sept. 2018, pp. 265–267.

[xviii] Tridello, A., Ciardiello, R., Paolino, D. S., & Goglio, L. (2020). Fatigue response up to 10^9 cycles of a structural epoxy adhesive. *Fatigue & Fracture of Engineering Materials & Structures, 43*(7), 1555–1566.

[xix] A. Tridello, D. S. Paolino, G. Chiandussi, and L. Goglio, "An innovative testing technique for assessing the VHCF response of adhesively bonded joints," *Fatigue & Fracture of Engineering Materials & Structures*, vol. 42, no. 1, pp. 84–96, 2019.

[xx] J. D. Berrio, "Characterization of effective Young's modulus for Fused Deposition Modeling manufactured topology optimization designs," *The International Journal of Advanced Manufacturing Technology*, Aug. 2019.

[xxi] ASTM E1876 / EN 843-2 (Impulse Excitation) and standard IET literature for bar specimens—methods for measuring elastic modulus and resonant frequencies.

[xxii] Adams, R. D., & Wake, W. C. *Structural Adhesive Joints in Engineering.* Elsevier (Butterworth-Heinemann), classic text on thickness, peel, and edge effects in bonded joints.

[xxiii] Moroni, F., *et al.* (2023). *Influence of high frequency on the fatigue life of metallic single-lap joints.* (preprint/article; versions appear 2023–2024).